

ISOTOPIC AND PETROLOGIC INVESTIGATION AND MODEL OF GENESIS OF  
LARGE-VOLUME HIGH-SILICA RHYOLITES IN ARC ENVIRONMENTS:  
KARYMSHINA CALDERA, KAMCHATKA, RUSSIA

by

NICCOLE KIYOMI SHIPLEY

A THESIS

Presented to the Department of Geological Sciences  
and the Graduate School of the University of Oregon  
in partial fulfillment of the requirements  
for the degree of  
Master of Science

December 2011

THESIS APPROVAL PAGE

Student: Niccole Kiyomi Shipley

Title: Isotopic and Petrologic Investigation and Model of Genesis of Large-Volume High-Silica Rhyolites in Arc Environments: Karymshina Caldera, Kamchatka, Russia

This thesis has been accepted and approved in partial fulfillment of the requirements for the Master of Science degree in the Department of Geological Sciences by:

Dr. Ilya Bindeman	Chairperson
Dr. Paul Wallace	Member
Dr. Mark Reed	Member

and

Kimberly Andrews Espy	Vice President for Research & Innovation/Dean of the Graduate School
-----------------------	--

Original approval signatures are on file with the University of Oregon Graduate School.

Degree awarded December 2011

© 2011 Niccole Kiyomi Shipley

## THESIS ABSTRACT

Niccole Kiyomi Shipley

Master of Science

Department of Geological Sciences

December 2011

Title: Isotopic and Petrologic Investigation and Model of Genesis of Large-Volume High-Silica Rhyolites in Arc Environments: Karymshina Caldera, Kamchatka, Russia

Large-volume calderas are responsible for producing large deposits of rhyolite and high-silica rhyolite, but the mechanisms by which these deposits are produced are still poorly understood. The Kamchatka Peninsula of Russia contains several large calderas and is one of the most volcanically active areas on Earth. Karymshina Caldera, the largest (25 km x 15 km) caldera in Kamchatka, produced an estimated 800 km<sup>3</sup> of high-silica rhyolitic ignimbrites and post-caldera extrusions, which erupted 1.78 and 0.5 – 0.8 Ma, respectively.

SiO<sub>2</sub> content ranges from 66.27-71.89 wt% in the ignimbrites and 70.16-77.70 wt% in the post-caldera extrusions studied. Crystal content is primarily quartz and plagioclase, 0.5-2 mm in size, with other minerals. Values of  $\delta^{18}\text{O}$ ,  $\delta\text{D}$ ,  $^{87}\text{Sr}/^{86}\text{Sr}$ , and  $^{144}\text{Nd}/^{143}\text{Nd}$  indicate little assimilation of crustal material, in contrast to modeling results. XRF analysis indicates a homogeneous magma. The rhyolite-MELTS program was used to model crystallization of a basaltic source with addition of amphibolite partial melt and hydrothermally-altered silicic rock to reproduce the observed compositions.

This thesis includes both previously published and co-authored material.

## CURRICULUM VITAE

NAME OF AUTHOR: Niccole Kiyomi Shipley

### GRADUATE AND UNDERGRADUATE SCHOOLS ATTENDED:

University of Oregon, Eugene, OR  
University of Minnesota, Minneapolis, MN  
Century Community College, White Bear Lake, MN

### DEGREES AWARDED:

Master of Science, Geology, 2011, University of Oregon  
Bachelor of Arts, Geology, 2007, University of Minnesota  
Associate of Arts, 1998, Century Community College

### AREAS OF SPECIAL INTEREST:

Volcanology  
Geochemistry  
Petrology

### PUBLICATIONS:

Bindeman IN, Leonov VL, Izbekov PE, Ponomareva VV, Watts KE, Shipley NK, Perepelov AB, Bazanova LI, Jicha BR, Singer BS, Schmitt AK, Portnyagin MV, and Chen CH (2010) Large-volume silicic volcanism in Kamchatka: Ar-Ar and U-Pb ages, isotopic, and geochemical characteristics of major pre-Holocene caldera-forming eruptions. *J Volcanol Geotherm Res* 189:57-80

## ACKNOWLEDGMENTS

I extend my deepest appreciations to Dr. Ilya Bindeman, Dr. Paul Wallace, and Dr. Mark Reed for their comments and assistance in preparing this manuscript as well as their patience with all my questions. This research was supported in part by a grant from the National Science Foundation, “Understanding the diverse isotopic record of volcanism in Kamchatka,” and a Career grant, “Stable Isotope Insights into large volume volcanic eruptions,” both awarded to Dr. Ilya Bindeman at the University of Oregon.

## TABLE OF CONTENTS

Chapter	Page
I. INTRODUCTION .....	1
Large-Volume Calderas and the Environments Where They Occur .....	2
Composition of Erupted Products and High-Silica Rhyolites (HSR).....	4
Petrogenetic Models of HSR Genesis.....	6
The Kamchatka Peninsula.....	12
II. KARYMSHINA CALDERA.....	18
History.....	18
Origin of Karymshina Caldera.....	18
III. METHODS .....	29
Volcanic Rocks of Karymshina Caldera.....	29
Whole Rock Chemistry.....	30
Mineralogy and Petrography.....	30
Isotope Analysis.....	36
IV. RESULTS .....	39
Whole Rock Chemistry.....	39
Geochronology.....	40
Mineralogy from Thin Sections .....	43
Ignimbrites .....	43
Post-Caldera Extrusions.....	46
Isotope Analysis.....	47

Chapter	Page
Oxygen Isotopes ( $\delta^{18}\text{O}$ ) .....	47
Hydrogen Isotopes ( $\delta\text{D}$ ).....	49
$^{87}\text{Sr}/^{86}\text{Sr}$ Isotope Ratios .....	50
$^{144}\text{Nd}/^{143}\text{Nd}$ Isotope Ratios.....	52
V. MELTS MODELING .....	54
Methods.....	54
Results.....	56
VI. DISCUSSION.....	66
Conclusions.....	71
REFERENCES CITED.....	73



## LIST OF FIGURES

Figure	Page
1. World map showing the location and size of several large calderas identified by Hughes and Mahood, (2008) with greater than 63 wt% SiO <sub>2</sub> .....	3
2. Karymshina Caldera as compared to a selection of subduction zone calderas throughout the world.....	5
3. A comparison of crustal thickness with SiO <sub>2</sub> content for the selection of subduction zone calderas of figure 2. ....	7
4. Schematic diagrams of the three main hypotheses for formation of HSR magmas. A) Formation of a deep crustal hot zone by the intrusion of mantle-derived basaltic sills into the lower crust. B) Crystal mush at various depths within the crust. C) Crustal underplating as basaltic sills from the mantle and lower crust heat overlying shallow crust beneath the caldera forming a magma chamber containing partial melts of crustal material only. D) Crustal recycling and remelting with addition of hydrothermally-altered material.....	9
5. Map of the Kamchatka Peninsula showing the locations of known volcanoes and caldera complexes dating from the Pleistocene through the Holocene.....	13
6. Map showing the isodepths to the subducting plate under the Kamchatka Peninsula in km (dotted lines).....	15
7. Graph showing a comparison of Karymshina Caldera samples to samples from a selection of arc settings, including the Kamchatka Arc.....	17
8. Map and cross-section of Karymshina Caldera, adapted from Leonov & Rogozin, (2007). The location of samples are shown as colored dots as indicated. The location of samples dated by Sheimovich and Golovin, (2003) are shown by the red letters and correspond to their dates in Table 1. ....	19
9. Image of a glacially eroded outcropping of the 1,000 m thick intra-caldera ignimbrite sheet.....	22
10. A) Map of the Kamchatka Peninsula showing the location of volcanic centers compared in a cross-section from fore-arc to back-arc. B) Graph comparing Karymshina Caldera to other calderas located in a cross-section of the Kamchatka Peninsula, moving away from the subduction zone trench. ....	41
11. Images of various phenocrysts and xenocrysts from thin section samples of Karymshina Caldera.....	44

Figure	Page
12. The results of crystallization experiments for the three most common island arc series (Normal- $\delta^{18}\text{O}$ ) with a comparison to the Karymshina Caldera samples.....	49
13. A graph comparing $\delta\text{D}$ values vs. wt% $\text{H}_2\text{O}$ for biotites and amphiboles from caldera-forming ignimbrites at Karymshina Caldera to other samples from the Eastern Volcanic Front. ....	51
14. An approximate mixing trend for $^{87}\text{Sr}/^{86}\text{Sr}$ and $^{144}\text{Nd}/^{143}\text{Nd}$ with an average crustal and mantle magma from the Kamchatka Peninsula as compared to caldera-forming ignimbrites from Karymshina Caldera.....	53
15. Graphs for selected compositional variables comparing the three possible starting compositions for use in rhyolite-MELTS modeling. ....	55
16. Results of equilibrium crystallization modeling at various pressures using the rhyolite-MELTS program. Results are shown for 0 wt% $\text{H}_2\text{O}$ and 2.5 wt% $\text{H}_2\text{O}$ in the initial melt composition. ....	57
17. Results of fractional crystallization modeling at 2 kbar using the rhyolite-MELTS program. Results are shown for 0 wt% $\text{H}_2\text{O}$ in the initial melt composition.....	59
18. Results of fractional crystallization modeling at 2 kbar using the rhyolite-MELTS program. Results are shown for 2.5 wt% $\text{H}_2\text{O}$ in the initial melt composition.....	60
19. Results of fractional crystallization modeling at 8 kbar using the rhyolite-MELTS program. Results are shown for 0 wt% $\text{H}_2\text{O}$ in the initial melt composition.....	61
20. Results of fractional crystallization modeling at 8 kbar using the rhyolite-MELTS program. Results are shown for 2.5 wt% $\text{H}_2\text{O}$ in the initial melt composition.....	62
21. Results of fractional crystallization modeling starting at 8 kbar and changing to 2 kbar at 50 wt% crystallization using the rhyolite-MELTS program. Results are shown for 0 wt% $\text{H}_2\text{O}$ in the initial melt composition.....	63
22. Results of fractional crystallization modeling starting at 8 kbar and changing to 2 kbar at 50 wt% crystallization using the rhyolite-MELTS program. Results are shown for 2.5 wt% $\text{H}_2\text{O}$ in the initial melt composition.....	64

Figure	Page
23. A diagram showing the normal values of $\delta^{18}\text{O}$ in various rock types. Karymshina Caldera falls within the normal range for HSR magmas.....	67
24. Graph of Rb vs. Sr for Karymshina Caldera and a cross-section of the Kamchatka Peninsula.....	69

LIST OF TABLES

Table	Page
1. Mineral and whole rock ages for samples from Karymshina Caldera.....	20
2. Summary of thin-section analyses, including electron-microprobe analysis of individual plagioclase, amphibole, and oxide phenocrysts and spot analyses of the glass matrix. ....	23
3. XRF and ICP-MS analyses of samples from Karymshina Caldera. ....	31
4. Results of various isotope studies by sample for Karymshina Caldera rocks. The calculated magma value of $d^{18}O$ was calculated according to formulas in Bindeman & Valley, (2002) and Bindeman, (2004) and whenever possible, the calculated magma values from quartz and from plagioclase were averaged.....	37
5. Compositions of the starting magma and assimilants used in the rhyolite-MELTS models. ....	56

## CHAPTER I

### INTRODUCTION

The formation of magmas with rhyolitic (70 – 74 wt% SiO<sub>2</sub>) and high-silica rhyolitic (greater than 74 wt% SiO<sub>2</sub>) compositions is currently a topic of debate in the geologic community (Bachmann & Bergantz, 2004, 2008; Annen et al., 2006; Watts et al., 2011). Several processes by which these magmas can form have been presented and all of these processes may be at work in different environments. The four main hypotheses for production of rhyolitic magmas are 1) fractional crystallization of a basaltic parent, 2) extraction of evolved melt from a crystalline mush, 3) underplating and crustal melting, and 4) recycling and remelting of crustal and previously erupted material due to intrusion of basaltic sills. These processes are of particular concern in the case of large-volume calderas. This is because these calderas tend to produce rhyolitic magmas which are more viscous and therefore erupt more explosively than their basaltic counterparts.

This study focuses on a series of rhyolites and high-silica rhyolites (referred to below as HSR) erupted from what has long been recognized as a volcano-tectonic depression and which was recently reinterpreted by Leonov and Rogozin (2007) as a large-volume caldera which they named Karymshina Caldera. As the rhyolites (all caldera-forming ignimbrites) and the HSR (post-caldera extrusions) appear to be a chemically continuous sequence of crystallization from one magma source and the surrounding volcanoes are basaltic in composition and therefore provide a reasonable estimate of the starting composition for the magma, Karymshina Caldera provides an ideal suite for testing of various methods of magma generation.

In this study, I provide mineralogical and chemical descriptions of the caldera-forming ignimbrites and post-caldera extrusions along with analysis of oxygen and hydrogen isotopes. I then compare this information with the results of rhyolite-MELTS modeling of the formation of the HSR magma at Karymshina Caldera.

This study further supports the interpretation of Leonov and Rogozin (2007) that the volcano-tectonic depression at Karymshina is actually a large volume caldera. Because there is no topographical expression of Karymshina Caldera, but the area still shows signs of volcanic activity, the area shows that identifying large-volume calderas based solely on topographical expression is a flawed method. Numerous large-volume calderas may be overlooked by this method and other techniques should also be developed and employed to identify these calderas throughout the world.

A portion of this work has been published in volume 189 of the Journal of Volcanology and Geothermal Research in January of 2010. I.N. Bindeman and V. L. Leonov performed preliminary XRF and oxygen isotope analyses of the rocks and dated several samples as noted in the appropriate chapters. I performed additional XRF and oxygen isotope analyses and  $^{87}\text{Sr}/^{86}\text{Sr}$  and  $^{144}\text{Nd}/^{143}\text{Nd}$  analyses.

### *Large-Volume Calderas and the Environments Where They Occur*

The processes by which large volumes of rhyolitic magma are generated worldwide is a topic of great debate (Jellinek and DePaolo, 2003; Geyer and Marti, 2008). Large-volume calderas often produce volumes of igneous rock that are greater than 500 km<sup>3</sup>, but there have been no such eruptions in human history so all the information we have related to what happens in large caldera eruptions is based on geologic study. In a

global survey of published studies, Hughes and Mahood (2008) found 91 calderas with diameters greater than 5 km and SiO<sub>2</sub> contents of at least 63 wt% (Fig. 1). Due to the number of large-volume calderas and because most calderas are formed by higher-silica, rhyolitic magmas it is important to understand the processes by which these calderas are formed. This includes examination of how such large volumes of magma with such high silica contents are created and stored prior to eruption.

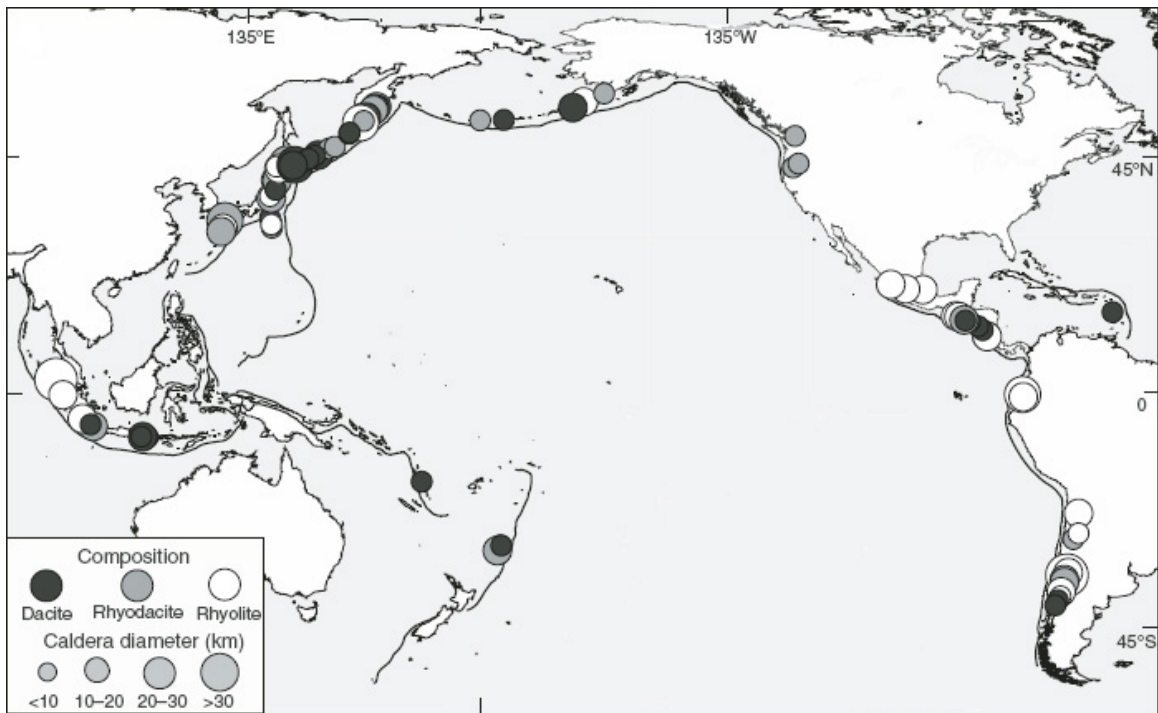


**Figure 1:** World map showing the location and size of several large calderas identified by Hughes and Mahood, (2008) with greater than 63 wt% SiO<sub>2</sub>. Figure is from their study.

In their compilation, Hughes and Mahood (2008) did not include calderas in complex arc environments, non-arc environments, and calderas not expressed visibly in the topography. Thus the actual number of large-volume calderas world-wide is higher than their estimate (represented in Fig. 1) and includes some particularly famous large-

volume eruptions, such as Long Valley and Yellowstone Calderas in the United States (Mahood et al., 2010; Bindeman & Valley, 2002; Shervais & Vetter, 2009; Cathey & Nash, 2009; Watts et al., 2010). While many large-volume calderas do occur in hotspots, especially continental hotspots, and transtensional environments, several studies have shown that they are commonly generated in subduction zones (Hughes and Mahood, 2008; Annen and Sparks, 2002; Annen et al., 2006; Ellis et al., 2007; Bindeman et al., 2010).

The subduction zones of the Pacific Ring of Fire are home to extensive volcanic activity. Many large and small-volume calderas are concentrated in these areas, particularly in areas of near-perpendicular collisions in continental margin arcs, as in the Andes Mountains of South America, Central America, and the Kamchatka Peninsula of Russia (Fig. 1).

#### *Composition of Erupted Products and High-Silica Rhyolites (HSR)*

Compositionally, there is a great range of magma compositions for large-volume eruptions worldwide (Fig. 2). Basaltic magmas with low-silica contents were erupted at Colli Albani in Italy (Giordano et al., 2006; Marra et al., 2009). On the high-silica end of the spectrum are calderas like Yellowstone Caldera and Long Valley Caldera, both in the United States (Mahood et al., 2010; Bindeman et al., 2006). 31 of the calderas identified in the Hughes and Mahood (2008) study produced rhyolites with at least 72 wt% SiO<sub>2</sub>, which is approximately 34 % of the calderas studied.

As with volcanism in general, the majority of high-silica rhyolitic (HSR) magmas (defined as having greater than 74 wt% SiO<sub>2</sub>) occur in hot spot environments and, to a



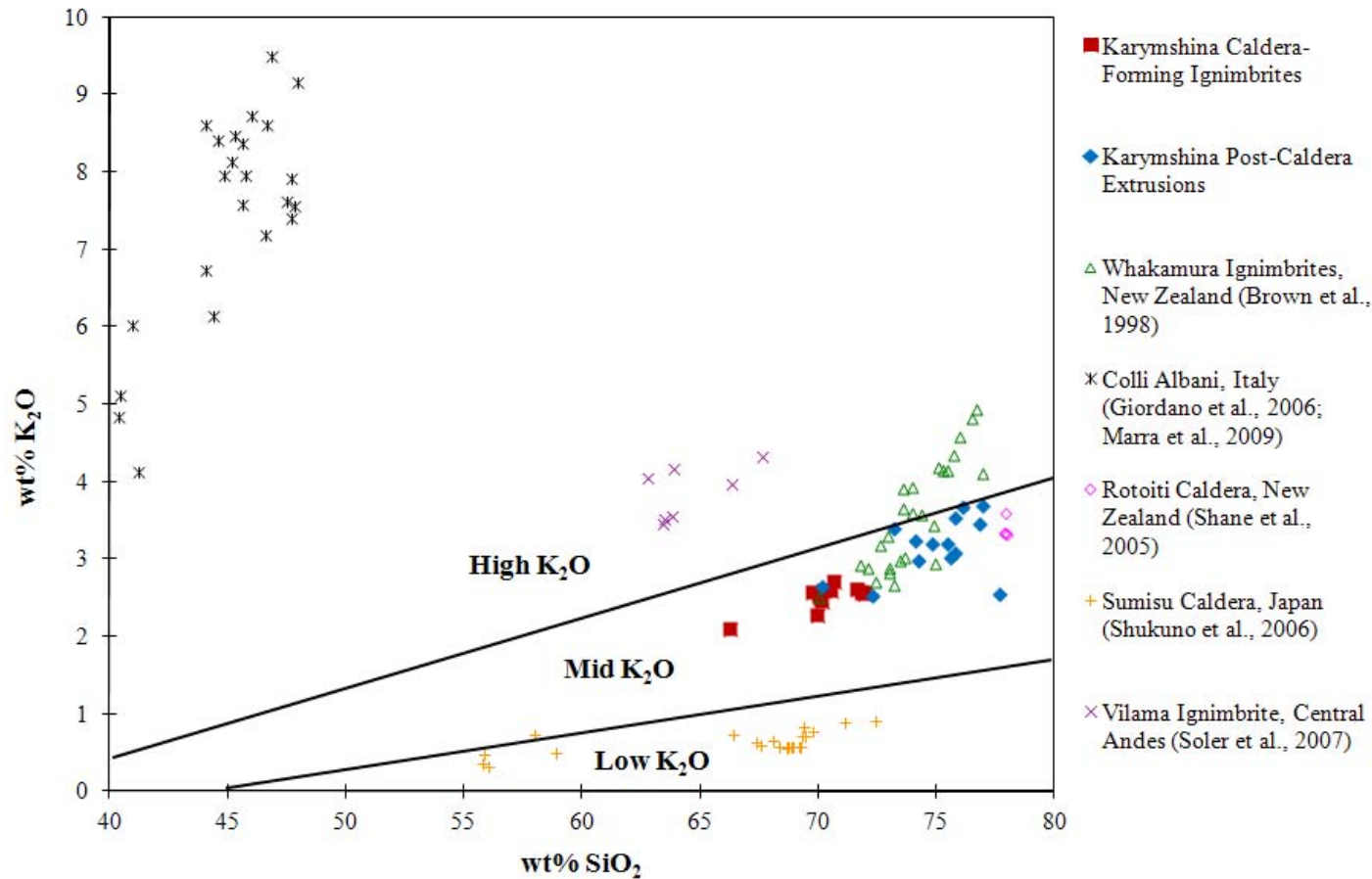


**Figure 2:** Karymshina Caldera as compared to a selection of subduction zone calderas throughout the world. Karymshina and the two calderas in New Zealand have high  $SiO_2$  contents, indicating that Karymshina is not completely unique in terms of the  $SiO_2$  content present in a subduction zone environment. Data for the additional selected calderas was taken from the sources indicated in the figure.

lesser degree, subduction zones, but have a higher tendency to form in areas of tension rather than compression within subduction zones (Hughes and Mahood, 2008). HSR magmas are also found at continental hot spots, such as at Yellowstone Caldera, and other volcanic areas of continental interiors rather than at oceanic hotspots (Fig. 1) (Mahood et al., 2010; Bindeman et al., 2006; Shervais & Vetter, 2009).

Although there is great variation in the overall composition of HSR magmas, in general they contain relatively low amounts of magnesium and iron and higher amounts of aluminum and potassium (Gunnarson et al., 1998; Brown et al., 1998; Shane et al., 2005), which is expected based on the common presence of plagioclase and alkali feldspars. HSR magmas in subduction zones also tend to have higher H<sub>2</sub>O contents (up to 6 wt%), a common feature of subduction zone magmas in general (Brown et al., 1998; Shane et al., 2005).

#### *Petrogenetic Models of HSR Genesis*

The most common interpretation of HSR magma genesis is that it is formed within large batholiths beneath the surface (Bachmann and Bergantz, 2004, 2008). The majority of HSR magmas contain few or no crystals and were the result of volcanic activity. HSR magmas are also in rare cases found as phaneritic intrusions (Bachmann and Bergantz, 2008; Hildreth, 2004).

Most HSR magmas are produced in areas of thicker crust and incorporate large amounts of continental crust, based on elevated <sup>87</sup>Sr/<sup>86</sup>Sr isotope ratios (Bindeman, 2008). Previous studies indicate that crust of at least 30 km in thickness is required to produce

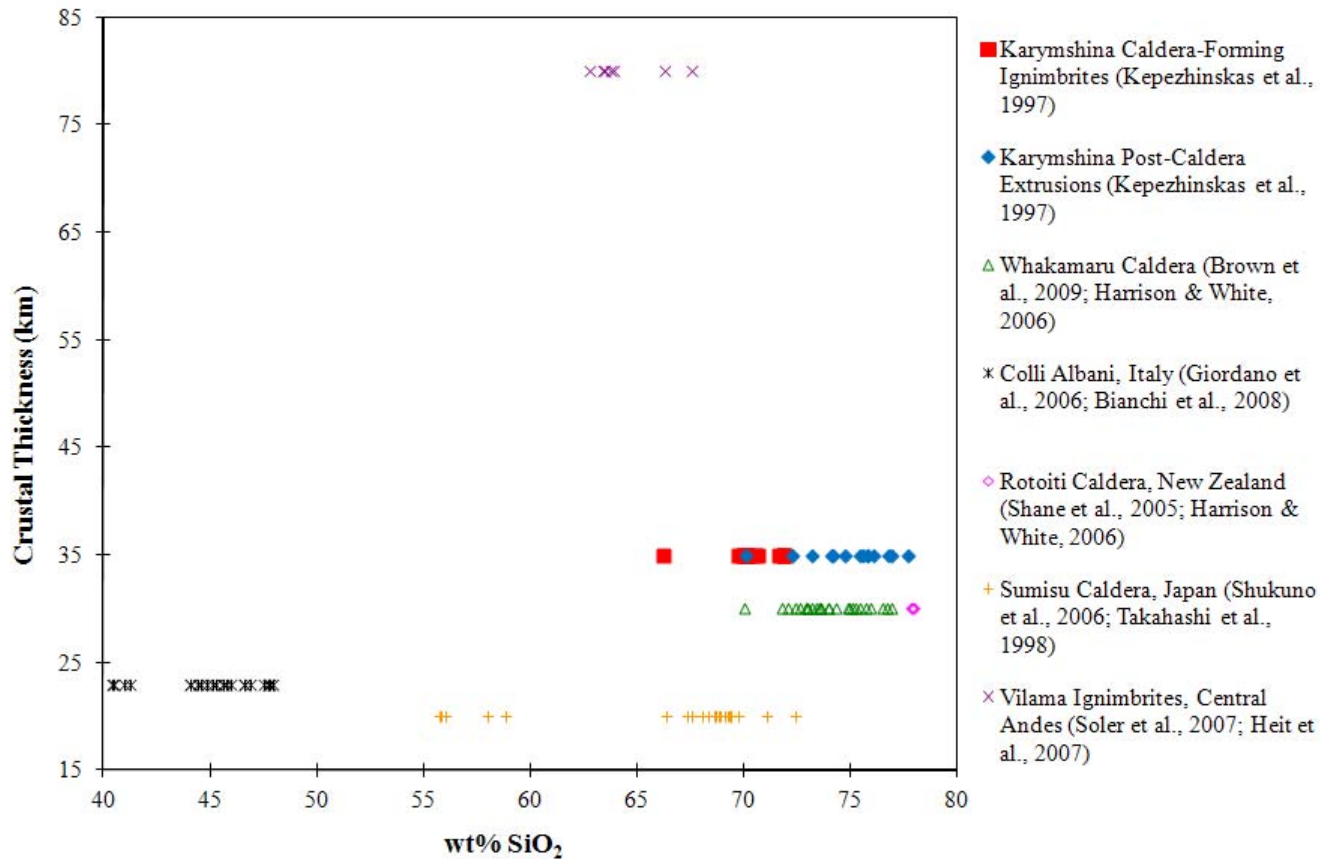


**Figure 3:** A comparison of crustal thickness with SiO<sub>2</sub> content for the selection of subduction zone calderas of figure 2. While low SiO<sub>2</sub> contents appear to correspond to thinner crust, there does not appear to be a correlation between crustal thickness and SiO<sub>2</sub> contents in HSR magmas. It is possible that in areas where the crust is thinner, delamination or some other process has thinned the crust after the HSR magmas were produced. Data for other calderas was taken from the sources indicated in the figure.

HSR magmas (Fig. 3) and 40 km is ideal (Hughes & Mahood, 2008). This requirement limits production of HSR magmas to areas of continental crust.

There are four currently accepted hypotheses regarding the production of HSR magmas (Fig. 4), 1) fractional crystallization of a basaltic parent in a deep crustal hot zone (Annen et al., 2006), 2) extraction of evolved melt from a crystalline mush (Bachmann and Bergantz, 2004), 3) underplating of basaltic sills from the mantle and crustal melting (Watts et al., 2011), and 4) recycling and remelting of crustal and previously erupted material (Watts et al., 2011). It is likely that the magma was formed by some combination of these four methods in most cases.

Fractional crystallization (Fig. 4a) of a basaltic parent magma is commonly accepted as a way to form HSR magmas as the first minerals to crystallize are olivines and pyroxenes, which causes the remaining melt to increase in SiO<sub>2</sub> content (Bowen, 1928; Annen et al., 2006). Basaltic magmas are also the primary magmas formed from melting of the mantle, thus early-formed magma in a subduction zone that results from flux of fluids through a hot mantle wedge will be basaltic in composition (Bachmann & Bergantz, 2008).

As basaltic magmas intrude at the base of the overlying crust and cool and crystallize, they form a deep crustal hot zone. Melts produced by fractional crystallization in this hot zone are enriched in SiO<sub>2</sub> and volatiles. Due to this increase in volatiles and SiO<sub>2</sub> the melt is more buoyant than the surrounding rock and rises through the crust (Annen et al., 2006; Annen & Sparks, 2002). A known issue with this method of forming HSR magmas is that the dense crystal cumulates that separated during fractional crystallization are not found in seismic and gravity studies. One explanation

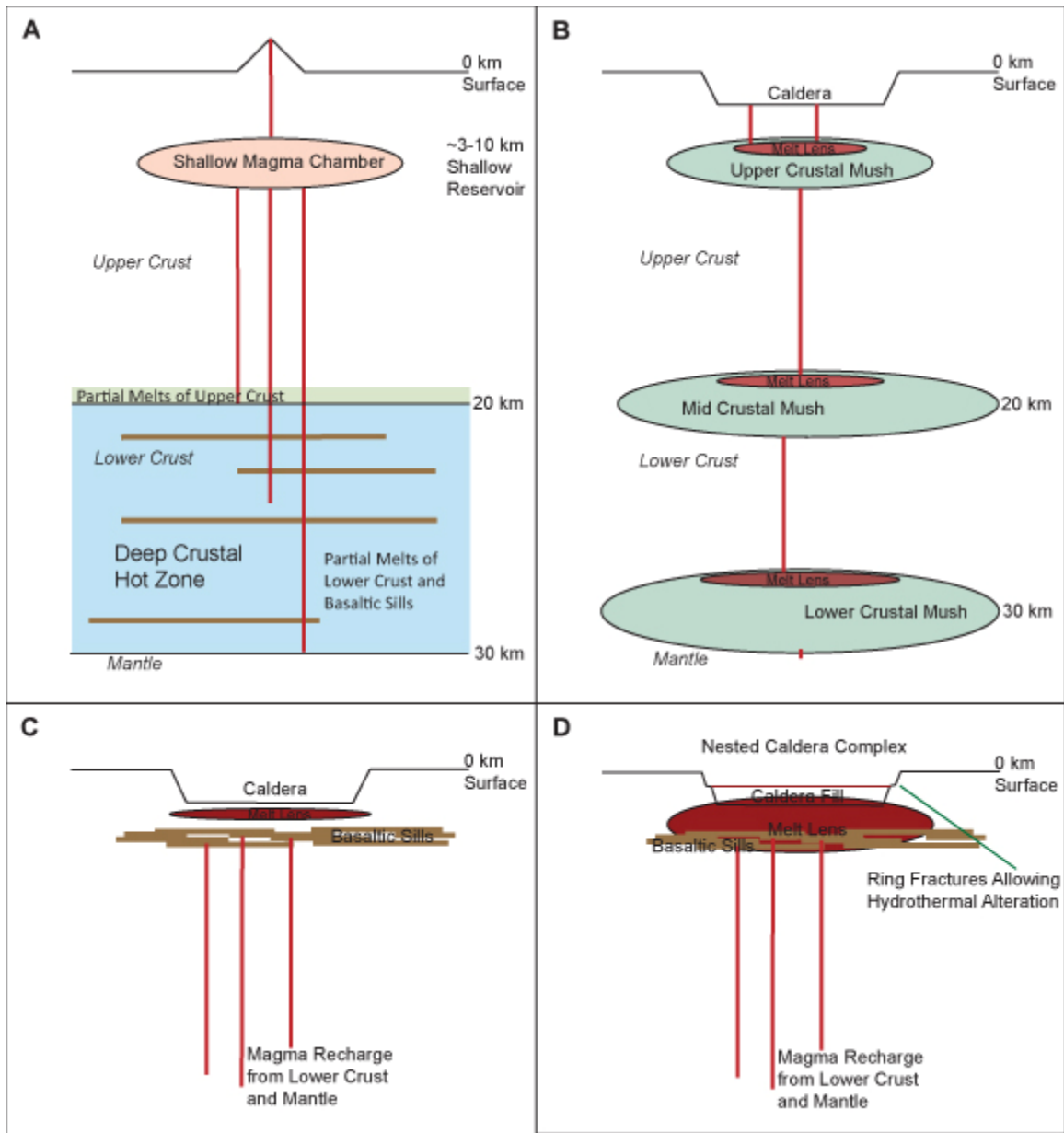


**Figure 4:** Schematic diagrams of the three main hypotheses for formation of HSR magmas. A) Formation of a deep crustal hot zone by the intrusion of mantle-derived basaltic sills into the lower crust. Sills partially melt surrounding crust while undergoing fractional crystallization and the resulting melt moves upward through buoyancy to the shallow crust. Adapted from Annen et al., (2006). B) Crystal mush at various depths within the crust. Magma undergoes fractional crystallization and buoyancy causes the residual melt to rise. Adapted from Bachmann and Bergantz, (2005). C) Crustal underplating as basaltic sills from the mantle and lower crust heat overlying shallow crust beneath the caldera forming a magma chamber containing partial melts of crustal material only. Adapted from Watts et al., (2011). D) Crustal recycling and remelting with addition of hydrothermally-altered material. Adapted from Watts et al., (2011).

for the absence of these dense cumulates is delamination of the lower crust (Annen et al., 2006). Approximately 60 % crystallization of a basaltic magma is required to obtain at least 60 wt% SiO<sub>2</sub> which means that the initial basaltic magma volume would need to be at least twice the volume of HSR magma produced (Annen et al., 2006; Bachmann & Bergantz, 2008). Modeling by Annen et al. (2006) has shown that it is possible to produce the required basaltic and HSR magma volumes seen in large-volume calderas by fractional crystallization of basaltic magmas in a deep crustal hot zone.

In the case of extraction of an evolved melt from a crystalline mush (Fig. 4b), the extraction may happen in lower, middle, or upper crustal levels (Bachmann and Bergantz, 2004). The crystalline mush is produced by rising magma that stalls when it reaches depths of equivalent rock density (Bachmann and Bergantz, 2004, 2008; Annen et al., 2006). The initial magma is produced in the mantle and intrudes the lower crust. As it cools and crystallizes, the melt is separated by crystal settling and compaction. The melt then rises until it stalls at a new depth and the process is repeated (Bachmann and Bergantz, 2004, 2008). Each new melt is enriched in SiO<sub>2</sub> and volatiles compared to the previous melt. In some cases the extraction of an evolved melt from a crystalline mush may be a completion of events that began with the fractional crystallization of basaltic magma in a deep crustal hot zone.

The extraction of evolved melt from a crystalline mush can occur by two methods 1) settling of crystals and 2) compaction of crystals (Bachmann & Bergantz, 2004). Both of these processes have been shown to require a long time ( $> 10^3$ - $10^6$  years), which would indicate that crystalline mushes could have a residence time on the order of millions of years in the shallow crust. Bachmann and Bergantz (2004) advocated that at 45-50 vol%

crystals, convection in the crystalline mush will cease and crystals will settle and compact at the bottom of the magma chamber, leaving the residual extracted melt close to the surface where it may continue crystallizing or erupt. These crystalline mushes can be remobilized by the intrusion of a small amount of magma rising from lower depths, which could provide enough mobilization and volatiles to cause an eruption (Bachmann & Bergantz, 2004). As with the fractional crystallization hypothesis, the original volume of magma must be approximately twice the erupted volume for HSR magmas, as evidenced by the required volume of crystals in the mush.

Crustal melting with underplating (Fig. 4c) again involves the intrusion of basaltic magma into the lower crust creating a deep crustal hot zone. However, in this case the basaltic magma remains separated from the crust, which forms the HSR magma. The heat from the intrusion of basaltic magmas (underplating) causes the melting of crustal material at a shallower level in the upper crust.

However, Annen & Sparks (2002) found that the heat generated in a deep crustal hot zone would cause the intruded basalts to come in direct contact with the crustal melt, likely causing mixing of the melts. At the same time, it is unlikely that an intruding basalt would not melt some of the crustal material into which it intruded (Annen et al., 2006), meaning that fractional crystallization alone is also not a likely method for producing HSR magmas. It is therefore most likely that a combination of fractional crystallization and crustal melting is needed to produce HSR magmas.

Generation of HSR magma by recycling and remelting of crustal material has been proposed in multi-caldera complexes (Fig. 4c, d) (Watts et al., 2010, 2011) where a relatively constant heat source below the caldera complex causes previously erupted

material within the caldera to remelt. The heat source in the crust comes from basaltic sills intruded from the mantle or lower crust. The erupted material of the caldera complex is reburied within the caldera and is exposed to hydrothermal alteration by meteoric water, which would lower  $\delta^{18}\text{O}$  values over time. This process would also tend to incorporate some of the basaltic sill complex at various stages in the magma evolution, though it would not be necessary for any particular magma batch. The incorporation to varying degrees of the basaltic sill complex would also allow for increases in  $\delta^{18}\text{O}$  values at varying points within an eruption sequence (Watts et al., 2011).

### *The Kamchatka Peninsula*

Due to high subduction convergence rates of 8 cm/yr (Gorbatov et al., 1999), the Kamchatka Peninsula of Russia is home to some of the most active volcanoes and largest calderas on Earth and therefore provides an excellent opportunity to study volcanoes and their formation. However, the remote location and, until recently, restrictions of the Soviet government have prevented extensive study in the area by international researchers. Recent studies have focused on the identification and characterization of large-volume calderas throughout this region (Braitseva et al., 1997; Bindeman et al., 2010 and references therein) as well as the study of other volcanoes, with the goal of understanding processes for formation of magma in the region (Duggen et al., 2007; Portnyagin & Bindeman, unpublished; Portnyagin et al., 2007; Portnyagin et al., 2009). Currently, there are at least 13 topographically expressed calderas in Kamchatka that have been identified and were active within the last 5.5 million years (Fig. 5) (Bindeman



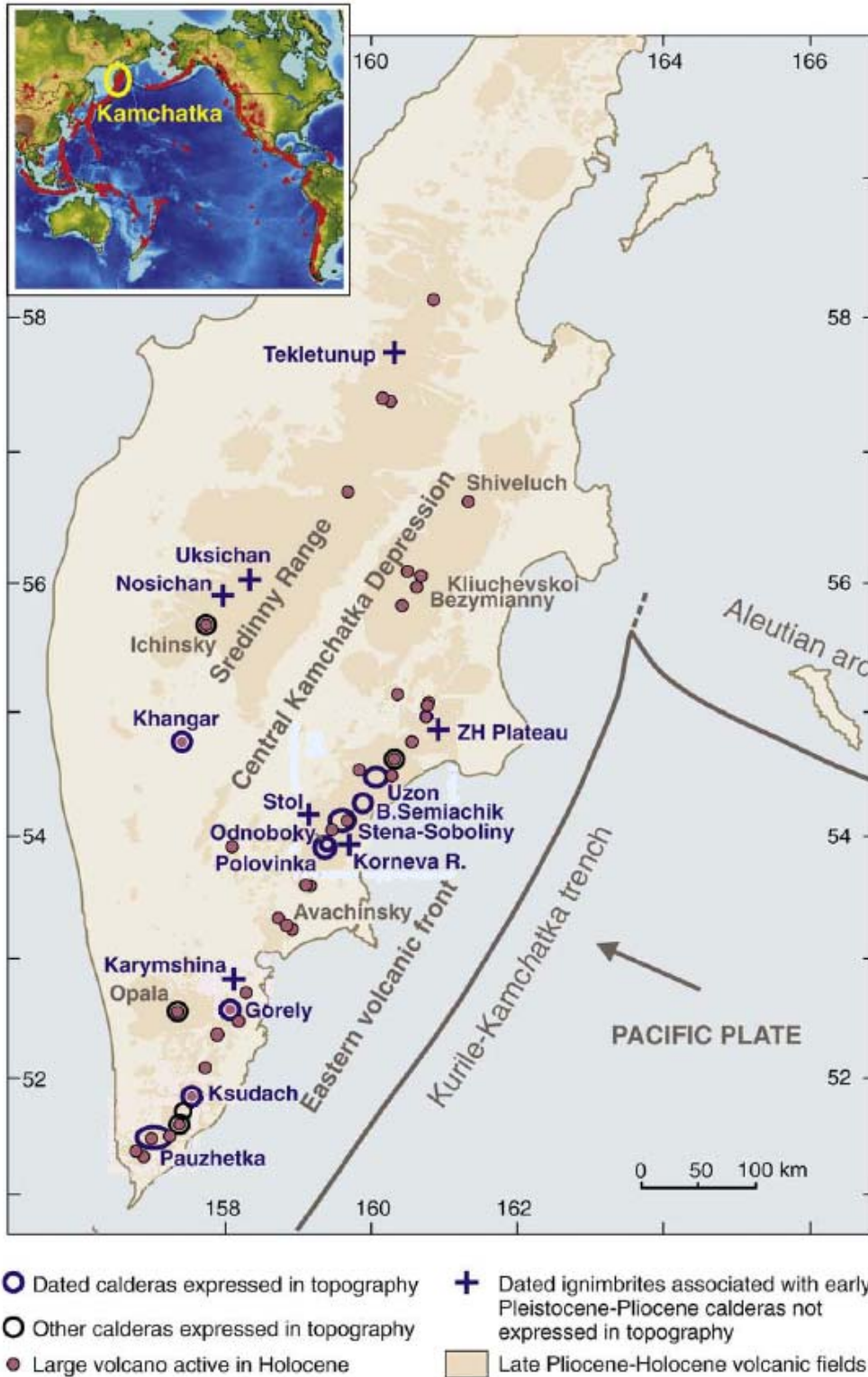


**Figure 5:** Map of the Kamchatka Peninsula showing the locations of known volcanoes and caldera complexes dating from the Pleistocene through the Holocene. Figure adapted from Bindeman et al., (2010).

et al., 2010). Most of these calderas are located in the southern half of the peninsula, where a subduction zone has existed since approximately 50 Ma (Scholl et al., 2007).

The current subduction zone along the eastern coast of the peninsula has been active since approximately 50 Ma (Scholl, 2007), but has migrated slowly as more crust has been accreted onto the peninsula's east coast. It runs parallel to the coastline from the southern tip of the peninsula to the Cape Kamchatka Peninsula (Scholl, 2007). Along this section of the subduction zone, which continues south into the Kurile Islands and Japan, the Pacific Plate is subducting nearly perpendicular to the peninsula. The depth to the subducting plate increases fairly rapidly moving away from the trench. Along the Eastern Volcanic Front (EVF), the depth ranges from 80-200 km (Fig. 6) (Nizkous et al., 2007; Auer et al., 2009). Under Karymshina Caldera (the focus of this study), the depth to the slab is approximately 130 km (Nizkous et al., 2007; Auer et al., 2009). The thickness of the continental crust across Kamchatka varies somewhat, but generally remains around 30-40 km thick in the central and southern segments (Fig. 6) (Kepezhinskias et al., 1997). The composition of the crust throughout the peninsula is composed of low to high-grade metamorphic rocks, including greenschist, blueschist, amphibolite, eclogite, and granulite. The southern half of the peninsula also contains a granulite-facies lower crust (Kepezhinskias et al., 1997). However, the surface of the peninsula contains large amounts of basalt and basaltic-andesite due to volcanic activity during the Holocene.

During the late Pleistocene and early Holocene, glaciers covered much of the Kamchatka Peninsula, varying somewhat in extent and location over time. These glaciers were alpine glaciers, unlike the continental glaciers present across North

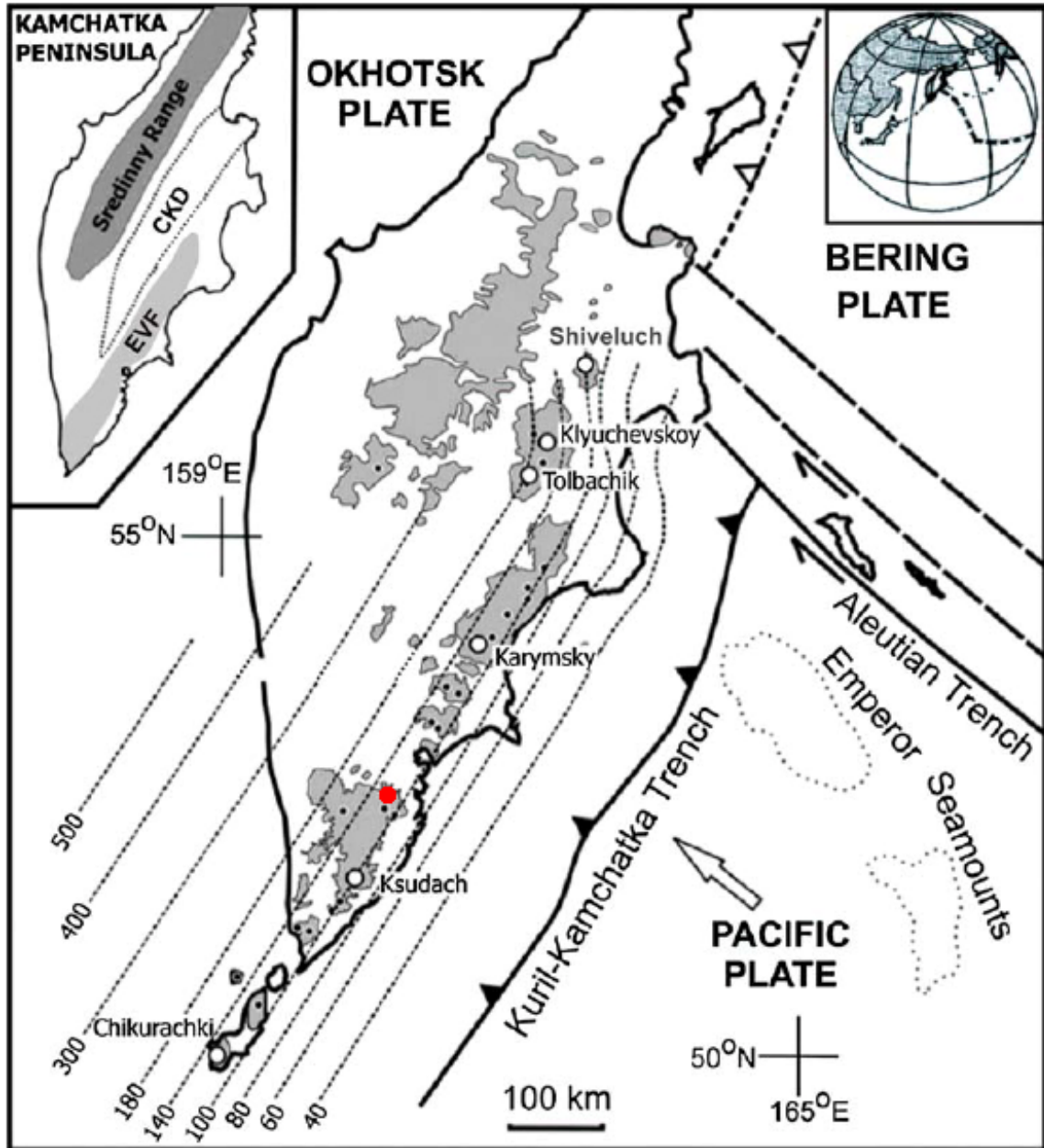


**Figure 6:** Map showing the isodepths to the subducting plate under the Kamchatka Peninsula in km (dotted lines). Grey areas are the main volcanic fields and black dots and open circles are currently active volcanoes. Karymskina Caldera is the red dot. Figure adapted from Auer et al., (2009).

America at the same time (Ponomareva et al., 2007). These glaciers caused extensive erosion of the landscape. Many of the calderas and volcanoes that existed prior to glaciation were eroded almost entirely, depending upon extent of glacial coverage in the

area. Volcanoes and calderas that became active during the glaciation have various degrees of erosion due to glacial activity (Ponomareva et al., 2007).

In the north and east of the peninsula is the Sredinny Range, which has few currently active volcanoes and several volcanoes that were active in the Late Pliocene to Mid-Pleistocene and are representative of the early volcanism in Kamchatka (Volynets, 1994; Ponomareva et al., 2007). Parallel to the southern half of the Sredinny Range and slightly west of it is the Central Kamchatka Depression (CKD), which is where some of the most active volcanoes are located (Bindeman et al., 2010; Ponomareva et al., 2007). The CKD is the most productive volcanic belt on the peninsula, despite having fewer volcanoes than both the Sredinny Range and the EVF (Ponomareva et al., 2007). As mentioned above, the majority of currently active volcanoes are located on the southern half of the peninsula, primarily in the EVF, which is located along the eastern edge of the peninsula and runs parallel to the CKD to the west of it (Fig. 5) (Bindeman et al., 2010; Ponomareva et al., 2007).

The majority of magmas produced on the Kamchatka peninsula are basaltic ranging from approximately 45-60 wt% SiO<sub>2</sub> as is true for most subduction zones worldwide (Fig. 7). HSR magmas constitute a minor portion of the magmas, consisting of roughly 2% of the total magma production on the peninsula, which is similar to other subduction zones (Bindeman et al., 2010; Hughes & Mahood, 2008; Ponomareva et al., 2007). Of the HSR magmas, the majority are found in large-volume calderas as opposed to other types of volcanoes (Fig. 2, 7). This is also true of HSR and rhyolitic magmas on the Kamchatka Peninsula and to Karymshina Caldera studied here (Fig. 7) (Bindeman et al., 2010).

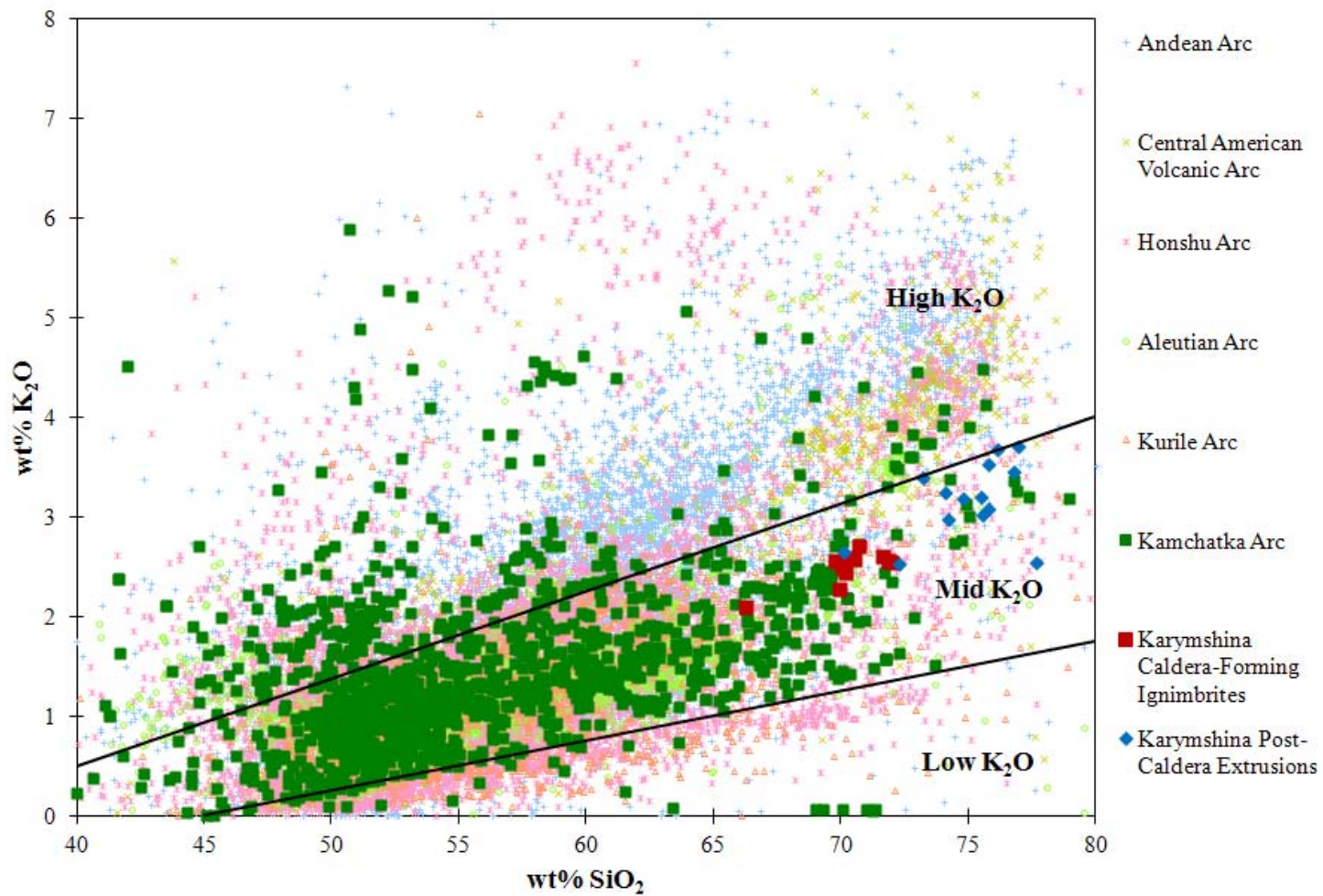


**Figure 7:** Graph showing a comparison of Karymshina Caldera samples to samples from a selection of arc settings, including the Kamchatka Arc. Data not from Karymshina Caldera is from the Georoc database at <http://georoc.mpch-mainz.gwdg.de/georoc>.

## CHAPTER II

### KARYMSHINA CALDERA

#### *History*

Karymshina Silicic Center is located on the Kamchatka Peninsula approximately 50 km southwest of the city of Petrapavlovsk-Kamchatsky (Fig. 5, 8). The caldera is roughly 25x15 km in size and the proposed caldera ring fractures are identified based upon outcrops of HSR and ignimbrite sheets in the area (Leonov & Rogozin, 2007). A great abundance of silicic rocks was noted during geologic mapping of the area in the 1960s and 1970s. The silicic rocks were initially considered to be extrusive in origin and the area was identified as a volcano-tectonic depression (Sheimovich & Khatskin, 1996; Sheimovich & Golovin, 2003). Leonov and Rogozin (2007) reinterpreted the silicic rocks as intracaldera deposits of ignimbrite and post-caldera extrusions. The identification of the Karymshina area as a caldera only occurred in 2007 owing to a lack of topographical expression of the caldera, a lack of extracaldera tuff deposits, and limited and difficult access to the remote location. It is still unclear whether the intracaldera ignimbrites represent a single eruption. However, Bindeman et al. (2010) used Ar-Ar dating of biotites in the top and bottom of the 1000 m thick intracaldera ignimbrite sheet and obtained identical ages of  $1.78 \pm 0.02$  Ma (Table 1).

#### *Origin of Karymshina Caldera*

The area surrounding Karymshina Caldera includes several hotspots and has long been identified as a volcano-tectonic depression (Leonov & Rogozin, 2007). It was initially believed that all the volcanic rocks in the area were related to extrusions and the

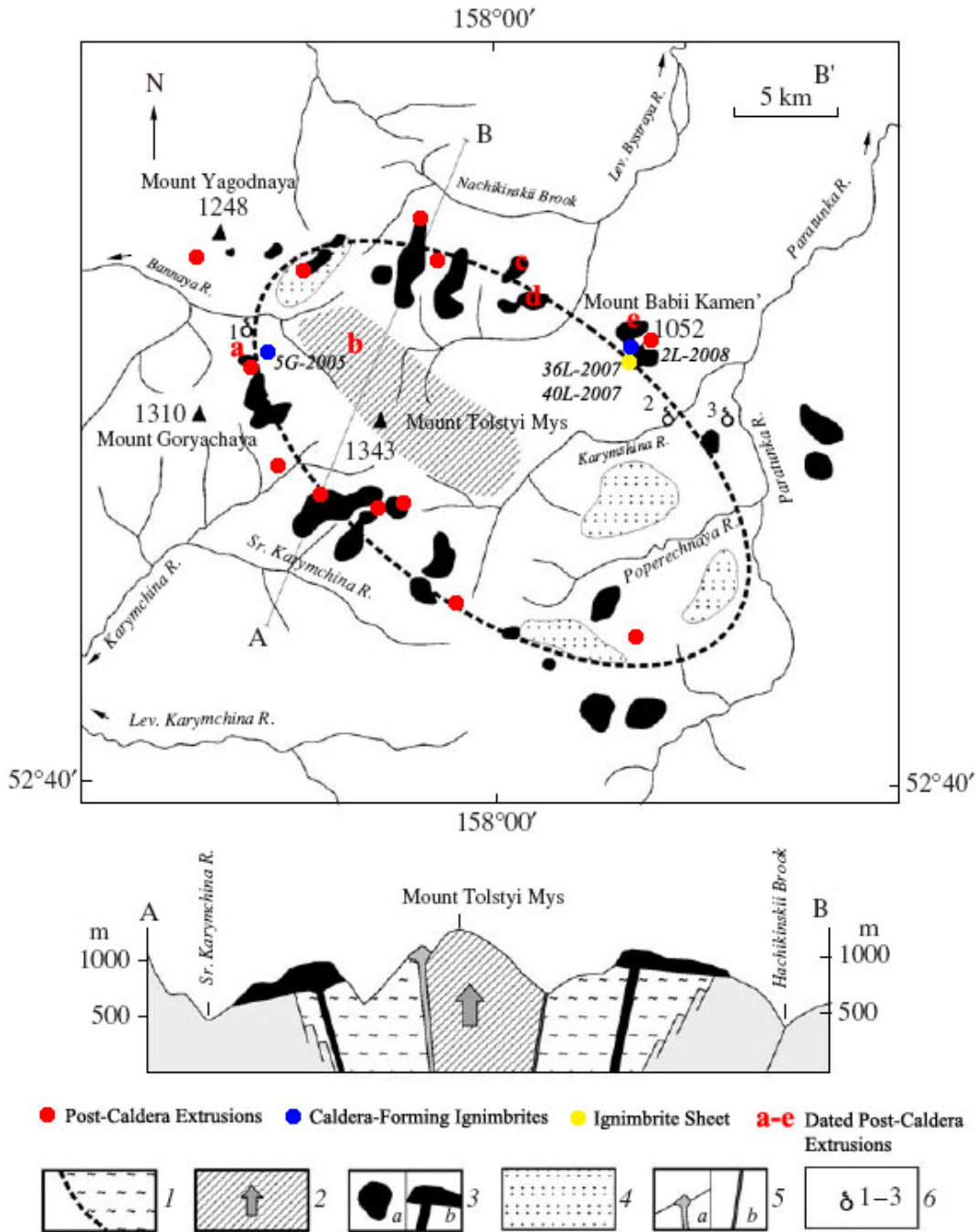


**Figure 8:** Map and cross-section of Karymshina Caldera, adapted from Leonov & Rogozin, (2007). The location of samples are shown as colored dots as indicated. The location of samples dated by Sheimovich and Golovin, (2003) are shown by the red letters and correspond to their dates in Table 1. 1: inferred boundary of caldera, with associated deposits, 2: resurgent uplift, 3: post-caldera extrusions, 4: lacustrine deposits, 5: small volcanic structures of basaltic lavas (a) and ore veins (b), 6: thermal springs; Bol'she-Bannaya (1), Karymshina (2), and Verkhne-Paratunka (3).

**Table 1:** Mineral and whole rock ages for samples from Karymshina Caldera. Data taken from sources as indicated below.

Sample Number	Additional Description	Plagioclase (Ar-Ar) or Whole Rock		Biotite (Ar-Ar)		Zircon (U-Pb)		Source
		Age $\pm$ My	MSWD (for Plagioclase)	Age $\pm$ My	MSWD	Age $\pm$ My	MSWD	
<i>Post-Caldera Extrusions</i>								
58L-2006		0.53 $\pm$ 0.05						Leonov & Rogozin, 2007
32L-2007						0.919 $\pm$ 0.084	0.26	Bindeman et al., 2010
2L-2008		0.50 $\pm$ 0.20						Leonov & Rogozin, 2007
a	Ar-Ar age	0.53 $\pm$ 0.05						Sheimovich & Golovin, 2003
b	Ar-Ar age	0.63 $\pm$ 0.03						Sheimovich & Golovin, 2003
c	Ar-Ar age	0.81 $\pm$ 0.02						Sheimovich & Golovin, 2003
d	Ar-Ar age	0.69 $\pm$ 0.02						Sheimovich & Golovin, 2003
e	Ar-Ar age	0.5 $\pm$ 0.2						Sheimovich & Golovin, 2003
<i>Caldera-Forming Ignimbrites</i>								
321L-1972		1.78						Leonov & Rogozin, 2007
5G-2005	Bannaya River	1.39 $\pm$ 0.10	1.12					
24L-2006		1.68 $\pm$ 0.30	0.38	1.78 $\pm$ 0.02	0.44	1.763 $\pm$ 0.090		Bindeman et al., 2010
36L-2007	Upper Portion of Ignimbrite Sheet	1.78				1.87 $\pm$ 0.11		Bindeman et al., 2010
40L-2007	Mid-Lower Portion of Ignimbrite Sheet	1.54 $\pm$ 0.09	0.34	1.78 $\pm$ 0.02	0.51			Bindeman et al., 2010



ignimbrite sheets in the depression came from eruptions of surrounding volcanoes (Sheimovich & Khatskin, 1996; Sheimovich & Golovin, 2003).

Leonov & Rogozin (2007) proposed that within the volcano-tectonic depression there is a large-volume caldera which they named Karymshina Caldera. The area of the caldera contains at least one ignimbrite sheet, which reaches exposed thicknesses of 1,000 m on the eastern edge and contains no observable stratigraphic differences (Fig. 9). Other outcrops of ignimbrite exist across the caldera and these may be the same ignimbrite deposit or other sheets, though compositionally they are identical. The ignimbrite outcrops wedge out as they approach the edges of the depression near the volcanoes Goryachaya, Yagodnaya, and Sunduk. The volcanic products of those volcanoes and additional large extrusions overlay the ignimbrite sheets along the supposed ring fracture, suggesting that the ignimbrites were produced by a different volcano (Fig. 8) (Leonov & Rogozin, 2007). The mineralogy of the ignimbrites from several locations across the proposed caldera is quite similar, containing phenocrysts of 16-21 vol% quartz, 19-25 vol% plagioclase, 0-4 vol% amphibole, 5-11 vol% biotite, and 1-3 vol% oxides with 42-48 vol% glass matrix (Table 2). The surrounding volcanoes, like Gorely and Mutnovsky, have produced only basalts and basaltic-andesites, while the ignimbrites and extrusions of the caldera are rhyolites (Bindeman et al., 2010; Leonov & Rogozin, 2007).

While there are extensive rhyolites within the proposed caldera, ignimbrites have not been found outside the caldera yet (Bindeman et al., 2010). The ignimbrite sheets within the caldera are weathered and, although they have some flow patterns, it still needs to be proven that the deposit is a single eruption. The lack of topographic expression for



**Figure 9:** Image of a glacially eroded outcropping of the 1,000 m thick intra-caldera ignimbrite sheet. The approximate location of three dated ignimbrite samples from the sheet are shown in yellow.

the caldera further complicates interpretations of the deposits. However, it is also possible, considering the age of the caldera, that glaciers and subsequent weathering and erosion have erased the extracaldera tuffs and topographical traces of the caldera rims. Examination of ash layers in ocean floor sediments has not identified any thick ash layers with an identical age to Karymshina Caldera at 1.78 Ma (Cao et al., 1995; Bindeman et al., 2010). While these studies have not found ash layers related to the caldera, the movement of the Pacific Plate subducting and the extent of ash fallout have not been estimated and taken into account. Evidence on the ocean floor may have already been subducted or, more likely, may be in a different area than expected.

**Table 2:** Summary of thin-section analyses, including electron-microprobe analysis of individual plagioclase, amphibole, and oxide phenocrysts and spot analyses of the glass matrix.

Sample Number	Additional Description	Glass (vol%)	Plagioclase Phenocryst	Analysis Location	Plag. (vol% for rock or wt% for phenocryst)	Quartz (vol%)
<i>Post-Caldera Extrusions</i>						
58L-2006		54			23	14
			1; Unzoned Phenocryst	Core	Ab <sub>73.15</sub> , An <sub>21.81</sub>	
				Rim	Ab <sub>71.12</sub> , An <sub>24.46</sub>	
			2; Concentric Zoning with Rim to Core Extinction	Core	Ab <sub>67.81</sub> , An <sub>28.48</sub>	
				Intermediate	Ab <sub>64.07</sub> , An <sub>32.69</sub>	
				Rim	Ab <sub>70.95</sub> , An <sub>24.66</sub>	
			3; Complex Core, Concentric Zoning Outside Core with Core to Rim Extinction	Core	Ab <sub>65.35</sub> , An <sub>31.39</sub>	
				Intermediate	Ab <sub>51.66</sub> , An <sub>46.63</sub>	
				Rim	Ab <sub>71.44</sub> , An <sub>24.09</sub>	
			4; Complex Core, Concentric Zoning Outside Core with Rim to Core Extinction	Core	Ab <sub>69.09</sub> , An <sub>27.02</sub>	
				Intermediate	Ab <sub>69.81</sub> , An <sub>26.15</sub>	
				Rim	Ab <sub>73.02</sub> , An <sub>22.16</sub>	
2L-2008		53			22	17

**Table 2:** continued

<b>Sample Number</b>	<b>Amphibole Phenocryst</b>	<b>Analysis Location</b>	<b>Amphibole (vol%)</b>	<b>Other (vol%)</b>
	<i>Post-Caldera Extrusions</i>			
58L-2006				Biotite-6, Oxides-3
2L-2008				Biotite-4, Oxides-2

**Table 2:** continued

Sample Number	Additional Description	Glass (vol%)	Plagioclase Phenocryst	Analysis Location	Plag. (vol% for rock or wt% for phenocryst)	Quartz (vol%)
<i>Caldera-Forming Ignimbrites</i>						
5G-2005	Bannaya River	43			46	2
24L-2006		42			25	21
36L-2007	Upper Portion of Ignimbrite Sheet	46	1; Semi-Concentric Zoning with Core to Rim Extinction	Core	Ab <sub>70.07</sub> , An <sub>25.89</sub>	20
				Intermediate	Ab <sub>69.80</sub> , An <sub>26.49</sub>	
				Rim	Ab <sub>67.80</sub> , An <sub>28.73</sub>	
			2; Semi-Concentric Zoning with Rim to Core Extinction	Core	Ab <sub>66.36</sub> , An <sub>30.39</sub>	
				Rim	Ab <sub>68.20</sub> , An <sub>28.43</sub>	
			3; Semi-Concentric Zoning with Core to Rim Extinction	Core	Ab <sub>67.83</sub> , An <sub>28.91</sub>	
				Intermediate	Ab <sub>67.19</sub> , An <sub>29.66</sub>	
				Rim	Ab <sub>68.67</sub> , An <sub>27.98</sub>	
			Xenocryst Plagioclase Phenocrysts		Ab <sub>38.19</sub> , An <sub>60.50</sub>	
40L-2007	Mid-Lower Portion of Ignimbrite Sheet	48	1; Unzoned Phenocryst	Core	Ab <sub>69.50</sub> , An <sub>26.90</sub>	16
				Rim	Ab <sub>66.73</sub> , An <sub>30.17</sub>	
			2; Complex Core, Unzoned Phenocryst	Core	Ab <sub>68.60</sub> , An <sub>28.00</sub>	
				Rim	Ab <sub>68.80</sub> , An <sub>27.80</sub>	
			3; Semi-Concentric Zoning with Rim to Core Extinction	Core	Ab <sub>71.50</sub> , An <sub>24.60</sub>	
				Intermediate	Ab <sub>72.23</sub> , An <sub>23.78</sub>	
				Rim	Ab <sub>72.03</sub> , An <sub>23.78</sub>	
			4; Semi-Concentric Zoning with Core to Rim Extinction	Core	Ab <sub>60.50</sub> , An <sub>37.20</sub>	
				Intermediate	Ab <sub>68.17</sub> , An <sub>28.43</sub>	
				Rim	Ab <sub>69.60</sub> , An <sub>27.10</sub>	

**Table 2:** continued

Sample Number	Amphibole Phenocryst	Analysis Location	Amphibole (vol%)
<i>Caldera-Forming Ignimbrites</i>			
5G-2005			5
24L-2006			4
36L-2007			2
	1; Amphibole with Amphicitic Rim	Core Rim	$K_{0.06}Ca_{1.73}Na_{0.13}Al_{0.07}Mg_{3.28}Mn_{0.14}Fe^{2+}_{1.01}Fe^{3+}_{0.53}Ti_{0.11}Si_{7.04}Al_{0.9597}O_{22}OH_{1.91}F_{0.08}Cl_{0.01}$ Formula could not be calculated
40L-2007			
			Biotite-11, Oxides-2, Xenocrysts

**Table 2:**  
continued

Sample Number	Glass Analysis (wt%)	SiO <sub>2</sub>	TiO <sub>2</sub>	Al <sub>2</sub> O <sub>3</sub>	FeO	MnO	MgO	CaO	Na <sub>2</sub> O
<i>Caldera-Forming Ignimbrites</i>									
5G-2005									
24L-2006									
36L-2007									
	1	75.645667	0.1190973	11.16109	0.816189	0.0187443	0.3735017	0.569472	2.7641267
	2	67.243367	0.119613	14.813467	1.5602747	0.012799	0.380218	0.8027013	3.41636
40L-2007									
	1	78.569467	0.0617513	11.024123	0.3688273	0.009595	0.0783313	0.6965777	3.59087
	2	53.2855	0.0433383	16.347667	0.3972237	0.0062117	0.0183603	0.656125	5.5103067

**Table 2:**  
continued

Sample Number	Glass Analysis (continued)	K <sub>2</sub> O	P <sub>2</sub> O <sub>5</sub>	S	Cl	F	O	Total
<i>Caldera-Forming Ignimbrites</i>								
5G-2005								
24L-2006								
36L-2007								
	1	4.68199	- 0.0047747	0.0045877	0.0127037	0.052693	-0.02506	96.19
	2	5.9867833	- 0.0007147	0.005262	0.0329783	- 0.0391867	0.00906	94.343
40L-2007								
	1	3.5107333	-0.00566	0.0030883	0.0132013	0.0394793	-0.0196	97.9408
	2	5.3679133	- 0.0070733	0.001318	0.021411	0.1593353	-0.07193	81.7357



## CHAPTER III

### METHODS

A portion of this work has been published in volume 189 of the Journal of Volcanology and Geothermal Research in January of 2010. I.N. Bindeman and V. L. Leonov performed preliminary XRF and oxygen isotope analyses of the rocks and dated several samples as noted. I performed additional XRF and oxygen isotope analyses and  $^{87}\text{Sr}/^{86}\text{Sr}$  and  $^{144}\text{Nd}/^{143}\text{Nd}$  analyses.

#### *Volcanic Rocks of Karymshina Caldera*

The volcanic rocks at Karymshina Caldera consist of ignimbrite sheets and post-caldera extrusions (Fig. 8, 9). Using the dimensions of the caldera and the volume of intracaldera ignimbrites ( $275 \text{ km}^3$ ) Leonov & Rogozin (2007) estimated that the eruptive volume was  $825 \text{ km}^3$  based on calculations presented by Mason et al. (2004). Most of this erupted material has been eroded away by glaciers, rivers, and general weathering in the wet climate of Kamchatka (Leonov & Rogozin, 2007).

Several samples of each rock type were taken in different areas of the caldera (Fig. 8) for analysis. In addition, samples were taken at the bottom, middle, and top of the outcropping portion of the 1,000 m thick ignimbrite sheet (Fig. 9). The samples analyzed in this study were collected in the field by Leonov and Rogozin in 2006, I.N. Bindeman in 2007, and N. Shipley in 2009.

### *Whole Rock Chemistry*

Table 3 presents whole rock chemical analyses of samples conducted in the studies of Leonov and Rogozin (2007) and Bindeman et al. (2010), as well as additional analyses previously not published. An initial set of x-ray fluorescence analyses (XRF) were performed on rock samples by Leonov and Rogozin. Additional samples were selected for analysis at Washington State University. The additional samples to be analyzed were selected based on location, with the intent of creating a picture of composition variation across the caldera. A subset of samples was analyzed to examine chemical variation within the 1,000 m ignimbrite sheet exposure. Samples of both ignimbrites and post-caldera extrusions were selected to determine the chemical variation between the two rock types. The results of these analyses were also used as a comparison to determine the accuracy of the earlier analyses of Leonov and Rogozin (2007), all of which are in agreement.

### *Mineralogy and Petrography*

Thin sections were made of five samples (2L-2008, 24L-2006, 36L-2007, 40L-2007, and 58L-2006) for electron microprobe analysis (Table 2, Fig. 8). An additional three covered thin sections were obtained from Vladimir Leonov (5G-2005, zh356, and zh423) and were examined with a petrographic microscope (Table 2). Three of the five microprobe thin sections and one of the covered thin sections are samples of ignimbrites. The remainder of the thin sections are samples of post-caldera extrusions. Samples were selected for thin section based on location within the caldera to provide sampling coverage across the caldera (Fig. 8). In addition, ignimbrite samples were chosen from

**Table 3:** XRF and ICP-MS analyses of samples from Karymshina Caldera. Data collected by 1-I. Bindeman, 2-S. Duggen, 3-V. Leonov. Some of the data were reported in Bindeman et al., (2010).

Sample Number Additional Description	Post-Caldera Extrusions						
	80L-2002	62L-2005	63L-2005	124L-2005	143L-2005	112L-2006	138L-2006
<b>XRF</b>							
<i>SiO<sub>2</sub></i>	75.49	76.13	75.82	74.23	76.81	76.98	72.32
<i>TiO<sub>2</sub></i>	0.204	0.120	0.190	0.217	0.149	0.145	0.282
<i>Al<sub>2</sub>O<sub>3</sub></i>	12.90	12.35	13.09	13.63	12.46	12.40	13.97
<i>FeO*</i>							
<i>Fe<sub>2</sub>O<sub>3</sub></i>	0.316	<0.1	<0.1	<0.1	<0.1	<0.1	0.402
<i>FeO</i>	1.510	0.985	1.440	1.860	1.290	1.150	1.680
<i>MnO</i>	0.0609	0.057	0.059	0.066	0.046	0.080	0.095
<i>MgO</i>	0.252	0.215	1.180	0.329	0.236	0.340	1.090
<i>CaO</i>	1.198	0.560	1.320	1.660	0.809	0.872	2.670
<i>Na<sub>2</sub>O</i>	3.845	3.750	3.940	4.021	3.727	3.700	3.730
<i>K<sub>2</sub>O</i>	3.197	3.680	3.080	2.980	3.450	3.700	2.530
<i>P<sub>2</sub>O<sub>5</sub></i>	0.0375	0.020	0.049	0.065	0.031	0.033	0.090
<i>Sum</i>	99.01	97.87	100.17	99.06	99.01	99.40	98.86
<i>SiO<sub>2</sub> Norm</i>							
<b>ICP-MS</b>							
<i>Ni</i>							
<i>Cr</i>							
<i>Sc</i>							
<i>V</i>							
<i>Ba</i>							
<i>Rb</i>							
<i>Sr</i>							
<i>Zr</i>							
<i>Y</i>							
<i>Nb</i>							
<i>Ga</i>							
<i>Cu</i>							
<i>Zn</i>							
<i>Pb</i>							
<i>La</i>							
<i>Ce</i>							
<i>Th</i>							
<i>Nd</i>							
<i>U</i>							
<b>Collected By</b>	3	3	3	3	3	3	3

**Table 3: Continued**

<b>Sample Number</b>	<b>Post-Caldera Extrusions</b>						
	32L-2007	35L-2007	56L-2007	80L-2007	81L-2007	82L-2007	105L- 2008
<b>Additional Description</b>							
<b>XRF</b>							
<i>SiO<sub>2</sub></i>	77.40, 62.91	73.22	74.80	75.60	74.10	75.80	77.70
<i>TiO<sub>2</sub></i>	0.180	0.184	0.502	0.239	0.371	0.154	0.102
<i>Al<sub>2</sub>O<sub>3</sub></i>	12.10	12.99	13.30	12.70	13.60	12.30	12.20
<i>FeO*</i>	1.62	1.23					
<i>Fe<sub>2</sub>O<sub>3</sub></i>			1.550	0.872	1.550	0.878	<.01
<i>FeO</i>			0.360	1.080	0.430	0.360	0.930
<i>MnO</i>	0.064	0.079	0.094	0.051	0.052	0.085	0.068
<i>MgO</i>	0.340	0.340	0.490	0.499	0.544	0.369	0.017
<i>CaO</i>	1.280	1.330	1.730	1.550	1.260	1.020	0.700
<i>Na<sub>2</sub>O</i>	3.240	3.960	3.640	3.260	4.120	3.520	3.810
<i>K<sub>2</sub>O</i>	3.200, 2.090	3.390	3.190	3.020	3.240	3.530	2.540
<i>P<sub>2</sub>O<sub>5</sub></i>	0.043	0.047	0.049	0.054	0.064	0.031	0.053
<i>Sum</i>	99.46	96.77	99.71	98.93	99.33	98.05	98.12
<i>SiO<sub>2</sub> Norm</i>	77.82	75.66					
<b>ICP-MS</b>							
<i>Ni</i>		0					
<i>Cr</i>		2					
<i>Sc</i>		4					
<i>V</i>		14					
<i>Ba</i>		909					
<i>Rb</i>		67					
<i>Sr</i>		143					
<i>Zr</i>		86					
<i>Y</i>		14					
<i>Nb</i>		3.9					
<i>Ga</i>		13					
<i>Cu</i>		1					
<i>Zn</i>		25					
<i>Pb</i>		11					
<i>La</i>		17					
<i>Ce</i>		31					
<i>Th</i>		5					
<i>Nd</i>		13					
<i>U</i>		3					
<b>Collected By</b>	2, 3	2	3	3	3	3	3

**Table 3: Continued**

<b>Sample Number</b>	<b>Caldera-Forming Ignimbrites</b>						
	5G-2005	24L-2006	36L-2007	37L-2007	38L-2007	39L-2007	40L-2007
<b>Additional Description</b>	Bannaya River		Upper Portion of Ignimbrite Sheet				Mid-lower Portion of Ignimbrite Sheet
<b>XRF</b>							
<i>SiO<sub>2</sub></i>	62.91, 62.90, 73.00	70.29, 72.80	70.55, 73.40	69.78	71.64	71.86	70.78, 73.00
<i>TiO<sub>2</sub></i>	0.625	0.287	0.283	0.299	0.295	0.296	0.290
<i>Al<sub>2</sub>O<sub>3</sub></i>	16.22	14.62	14.68	14.62	14.61	14.71	14.69
<i>FeO*</i>	4.57	2.25	1.63	1.94	1.32	1.38	2.70
<i>Fe<sub>2</sub>O<sub>3</sub></i>							
<i>FeO</i>							
<i>MnO</i>	0.116	0.090	0.039	0.041	0.042	0.064	0.096
<i>MgO</i>	1.650	0.760	0.680	0.650	0.560	0.510	0.600
<i>CaO</i>	4.650	2.790	2.300	2.570	2.490	2.380	2.330
<i>Na<sub>2</sub>O</i>	3.770	3.930	3.800	3.920	4.040	3.990	4.140
<i>K<sub>2</sub>O</i>	2.090	2.580	2.550	2.560	2.610	2.560	2.560
<i>P<sub>2</sub>O<sub>5</sub></i>	0.179	0.083	0.051	0.088	0.065	0.074	0.070
<i>Sum</i>	96.77	97.68	96.56	96.46	97.67	97.83	98.26
<i>SiO<sub>2</sub> Norm</i>	65.01	71.96	73.06	72.33	73.35	73.46	72.03
<b>ICP-MS</b>							
<i>Ni</i>	0	0	0	0	0	0	0
<i>Cr</i>	6	4	3	3	4	4	3
<i>Sc</i>	14	5	5	6	6	4	5
<i>V</i>	108	36	28	40	32	29	40
<i>Ba</i>	651	791	783	807	793	801	783
<i>Rb</i>	40	53	51	51	51	51	52
<i>Sr</i>	449	280	261	274	274	274	277
<i>Zr</i>	151	98	94	100	97	98	95
<i>Y</i>	21	15	12	13	12	13	13
<i>Nb</i>	2.9	2.5	1.7	2.3	3.3	2.9	1.8
<i>Ga</i>	17	12	14	14	13	13	13
<i>Cu</i>	24	5	5	5	4	3	5
<i>Zn</i>	62	35	27	37	23	25	30
<i>Pb</i>	8	7	8	8	9	8	8
<i>La</i>	12	12	12	13	10	15	13
<i>Ce</i>	23	26	24	24	22	28	23
<i>Th</i>	3	4	4	4	4	3	3
<i>Nd</i>	14	13	9	11	9	12	11
<i>U</i>	2	2	2	2	2	0	1
<b>Collected By</b>	2	1, 2	2, 3	2	2	2	2, 3

**Table 3: Continued**

<b>Sample Number</b>	<b>Caldera-Forming Ignimbrites</b>					
	41L-2007	43L-2007	44L-2007	45L-2007	46L-2007	47L-2007
<b>Additional Description</b>						
<b>XRF</b>						
<i>SiO<sub>2</sub></i>	70.00	70.20	70.19	70.71	70.10	69.95
<i>TiO<sub>2</sub></i>	0.292	0.282	0.287	0.279	0.286	0.288
<i>Al<sub>2</sub>O<sub>3</sub></i>	14.82	14.51	14.82	14.76	14.76	15.11
<i>FeO</i> *	2.75	2.05	2.30	2.09	2.24	2.31
<i>Fe<sub>2</sub>O<sub>3</sub></i>						
<i>FeO</i>						
<i>MnO</i>	0.098	0.092	0.100	0.056	0.061	0.095
<i>MgO</i>	0.770	0.760	0.740	0.670	0.740	0.690
<i>CaO</i>	2.300	2.690	2.700	2.460	2.640	2.790
<i>Na<sub>2</sub>O</i>	4.110	3.800	4.170	4.150	4.160	4.250
<i>K<sub>2</sub>O</i>	2.530	2.590	2.440	2.700	2.490	2.270
<i>P<sub>2</sub>O<sub>5</sub></i>	0.081	0.082	0.082	0.077	0.082	0.080
<i>Sum</i>	97.75	97.05	97.83	97.93	97.55	97.83
<i>SiO<sub>2</sub> Norm</i>	71.61	72.33	71.75	72.20	71.85	71.50
<b>ICP-MS</b>						
<i>Ni</i>	0	0	0	0	0	0
<i>Cr</i>	4	3	4	3	3	3
<i>Sc</i>	5	5	5	5	6	7
<i>V</i>	45	37	36	36	38	41
<i>Ba</i>	790	782	779	822	786	748
<i>Rb</i>	50	55	49	55	49	45
<i>Sr</i>	272	268	288	263	285	300
<i>Zr</i>	98	97	97	98	98	100
<i>Y</i>	12	12	13	14	12	13
<i>Nb</i>	2.4	2.7	2.2	2.4	2.4	1.9
<i>Ga</i>	14	14	13	14	13	14
<i>Cu</i>	5	5	5	4	5	4
<i>Zn</i>	41	33	41	35	33	37
<i>Pb</i>	7	9	14	8	6	7
<i>La</i>	9	11	15	15	12	12
<i>Ce</i>	22	29	23	26	22	24
<i>Th</i>	3	3	3	3	4	2
<i>Nd</i>	10	12	10	14	12	12
<i>U</i>	1	2	3	2	1	2
<b>Collected By</b>	2	2	2	2	2	2

both the top and bottom of the 1,000 m ignimbrite sheet to allow examination of changes within the ignimbrite sheet.

Electron microprobe analyses of thin sections (Table 2) were performed at the Lokey Laboratories, University of Oregon on the Cameca SX-100 using an accelerating voltage of 15 kV, a 30 nA beam current, and a 10  $\mu\text{m}$  spot beam size. Several plagioclase crystals were analyzed from each sample, as well as some amphiboles, plagioclase crystals within xenocrysts, and the glass matrix. Probed plagioclase crystals were chosen to represent a variety of zoning types; unzoned, complex, and concentric. In addition, plagioclase with core - rim and rim - core extinction patterns were selected. The amphiboles analyzed were chosen because they have exsolution rims. Plagioclase crystals were chosen at random within xenoliths to provide a sampling of xenolith crystal compositions and to examine differences in composition between the xenoliths and the extrusive rock matrix. Random selection of plagioclase crystals within the xenoliths was due to the small size of the crystals, which made features such as zoning impossible to see. The glass matrix was analyzed in several locations to check for potential variation within the matrix.

Spot analyses of the plagioclase crystals in the matrix were performed at least on the rim and in the core of the crystal. Some crystals also had spot analyses performed at other points within the crystal. Wherever possible, at least three spot analyses were taken at each location analyzed to increase accuracy of the results. Spot analyses of the amphiboles were performed at the core and within the exsolution rim. Plagioclase crystals within the xenocrysts were analyzed at the cores.

### *Isotope Analysis*

Oxygen isotopes were analyzed in plagioclase and quartz using samples weighing approximately 1.5 mg on the MAT 253 Stable Isotope Ratio Mass Spectrometer, a CO<sub>2</sub> laser fluorination vacuum line, at the University of Oregon. All analyzed crystals were checked under the microscope to ensure they were free of inclusions and lacked alteration due to weathering. The largest phenocrysts available were analyzed individually (Table 4) to check for isotopic variation among the phenocrysts. However, none were found and thus bulk analyses are robust.

Two samples from the Karymshina ignimbrites were analyzed by Cs primary beam using polished zircon mounts (also previously used for U-Pb dating, Table 1) at the UCLA ion microprobe facility on the Cameca 1270 ion microprobe and returned values of  $5.2 \pm 0.3$  permil.

Hydrogen isotopes were analyzed in biotite and amphibole using samples weighing approximately 1.5 mg on the High Temperature Conversion/Elemental Analyzer (TC/EA) coupled with the MAT 253 mass spectrometer at the University of Oregon. Only biotite and amphibole samples taken from the ignimbrites were analyzed as insufficient quantities of these minerals in an unaltered state were present in the post-caldera extrusions. All samples used were checked as described above to ensure that these phases were fresh and not chloritized or oxidized and were free of inclusions.

<sup>86</sup>Sr/<sup>87</sup>Sr and <sup>144</sup>Nd/<sup>143</sup>Nd ratios were analyzed at Central Washington University by Dr. Frank Ramos using TIMS. These data were obtained from whole rock powders. Samples were checked for alteration due to weathering prior to being powdered for analysis.



**Table 4:** Results of various isotope studies by sample for Karymshina Caldera rocks. The calculated magma value of  $d^{18}O$  was calculated according to formulas in Bindeman & Valley, (2002) and Bindeman, (2004) and whenever possible, the calculated magma values from quartz and from plagioclase were averaged.

Sample Number	Additional Description	dD in ‰ with H <sub>2</sub> O in wt%		Amph.	H <sub>2</sub> O in Amph.	d <sup>18</sup> O in ‰	d <sup>18</sup> O in ‰	d <sup>18</sup> O in ‰
		Biotite	H <sub>2</sub> O in Biotite			Quartz	Plag.	Cpx
<i>Post-Caldera Extrusions</i>								
107L-05						7.22		
124L-05						7.37 ± 0.21	6.38 ± 0.05	
143L-05						7.31	6.29	
49L-06							6.22	
58L-06						7.08 ± 0.05	6.36 ± 0.03	
75L-06						7.55 ± 0.15	6.39 ± 0.03	
88L-06						7.14	6.34	
112L-06						7.3	6.49	
138L-06						7.56	6.51 ± 0.07	
80L-07						7.23 ± 0.04	6.33 ± 0.11	
82L-2007						7.43	6.56 ± 0.01	
2L-08						7.16 ± 0.27	6.36	
<i>Caldera-Forming Ignimbrites</i>								
321L-1972								
2005G-5	Bannaya River						5.83, 5.76, 5.90	3.79, 4.09
23L-2006		-109.85	2.38					
24L-2006						7.50, 7.26	5.71	
36L-2007	Upper Portion of Ignimbrite Sheet	-124.87	2.58				6.53	
37L-2007		-119.00 (Altered)	2.68					
38L-2007		-120.82 (Altered)	2.56					
40L-2007	Mid-lower Portion of Ignimbrite Sheet	-141.22 (Altered)	2.67			7.91	6.33	
44L-2007		-113.67	2.10	-120.96	1.97			
45L-2007		-141.74	2.30					
47L-2007		-142.76	2.87	-148.89	1.83			
48L-2007						8.12, 7.75		

**Table 4: Continued**

Sample Number	Additional Description	d <sup>18</sup> O in ‰ Zircon	d <sup>18</sup> O in ‰ Calculated Magma Value	<sup>87</sup> Sr/ <sup>86</sup> Sr	10 <sup>-6</sup>	<sup>143</sup> Nd/ <sup>144</sup> Nd	10 <sup>-6</sup>	eNd	Source
<i>Post-Caldera Extrusions</i>									
107L-05			6.77						
124L-05			6.93						
143L-05			6.89						
49L-06									
58L-06			6.63						
75L-06			7.10						
88L-06			6.69						
112L-06			6.98						
138L-06			7.06						
80L-07			6.85						
82L-2007			7.07						
2L-08			6.71						
<i>Caldera-Forming Ignimbrites</i>									
321L-1972				0.703320	8	0.513015	12		
2005G-5	Bannaya River		6.17	0.703324	10	0.513065	12	8.29	Bindeman et al., 2010
23L-2006									
24L-2006			6.55						Bindeman et al., 2010
36L-2007	Upper Portion of Ignimbrite Sheet	4.71, 5.87 4.12, 4.75, 5.64, 6.12	7.02	0.703328	10	0.513048	12	7.96	Bindeman et al., 2010
37L-2007									
38L-2007									
40L-2007	Mid-lower Portion of Ignimbrite Sheet		7.14	0.703317	8				Bindeman et al., 2010
44L-2007									
45L-2007									
47L-2007									
48L-2007			7.49						

## CHAPTER IV

### RESULTS

A portion of this work has been published in volume 189 of the Journal of Volcanology and Geothermal Research in January of 2010. I.N. Bindeman and V. L. Leonov performed preliminary XRF and oxygen isotope analyses of the rocks and dated several samples as noted. I performed additional XRF and oxygen isotope analyses and  $^{87}\text{Sr}/^{86}\text{Sr}$  and  $^{144}\text{Nd}/^{143}\text{Nd}$  analyses.

#### *Whole Rock Chemistry*

The results of the XRF analyses show that both the caldera-forming ignimbrites and the post-caldera extrusions have high  $\text{SiO}_2$  and moderate  $\text{K}_2\text{O}$  (based on expected values compared to  $\text{SiO}_2$ ) content. The post-caldera extrusions are more differentiated and have higher  $\text{SiO}_2$  and  $\text{K}_2\text{O}$  than the ignimbrites, although none of the rocks contain phenocrysts of potassium feldspar. Comparison to values for other continental arc environments (data obtained from [www.georoc.com](http://www.georoc.com)) (Fig. 7) shows that the HSRs from Karymshina Caldera are consistent with the high end of compositional values present in both other arcs and other samples from the Kamchatka Peninsula. However, the HSR from Karymshina Caldera does appear to fit along a general trend of magma evolution within the arcs from primitive basalts to more evolved rhyolitic magmas. When compared with other large-volume calderas worldwide (Fig. 2), Karymshina Caldera appears to be relatively close in  $\text{SiO}_2$  and  $\text{K}_2\text{O}$  content. This, expectedly, indicates that large-volume calderas are more often produced from the most evolved silicic magmas. A comparison of the composition of volcanic rocks from Karymshina Caldera with volcanic

rocks from other volcanic centers in a cross-section of the subduction zone from fore-arc to back-arc (Fig. 10a, b) shows that Karymshina rhyolites have the highest values of SiO<sub>2</sub>, although there are a few samples which have similarly high SiO<sub>2</sub> and K<sub>2</sub>O values in the areas further from the trench, but none of the samples from volcanoes closer to the trench have values anywhere close.

### *Geochronology*

The eruption age of Karymshina Caldera is between 1.39 Ma (Ar-Ar dating of plagioclase) and 1.87 Ma (U-Pb dating of zircon) (Bindeman et al., 2010). Since zircon ages commonly record the time of zircon crystallization and can precede the eruption by 0.05 – 0.2 million years (Bindeman et al., 2006), the Ar-Ar ages are considered more reliable for the eruption age. Since the biotite Ar-Ar ages from two samples are identical at  $1.78 \pm 0.02$  Ma (Table 1) and unaltered biotite provides more accurate ages than plagioclase, the caldera-forming eruption age is assigned as  $1.78 \pm 0.02$  Ma. The dated samples were taken from across the caldera as well as the top and bottom of the 1,000 m outcropped ignimbrite sheet. Dates from the top and bottom of the ignimbrite sheet are in agreement within the resolution available, indicating that the sheet is likely from one eruption, or eruptions which occurred very close together. Our observation of the ignimbrite sheet has not shown any stratigraphic evidence of multiple eruptions such as layering of tephra and ignimbrite deposits with soil deposits, making it more likely that the sheet was produced in a single eruption. Dating of the post-caldera extrusions has yielded ages ranging from 0.5 – 0.8 Ma (Table 1) (Sheimovich and Khatskin, 1996;

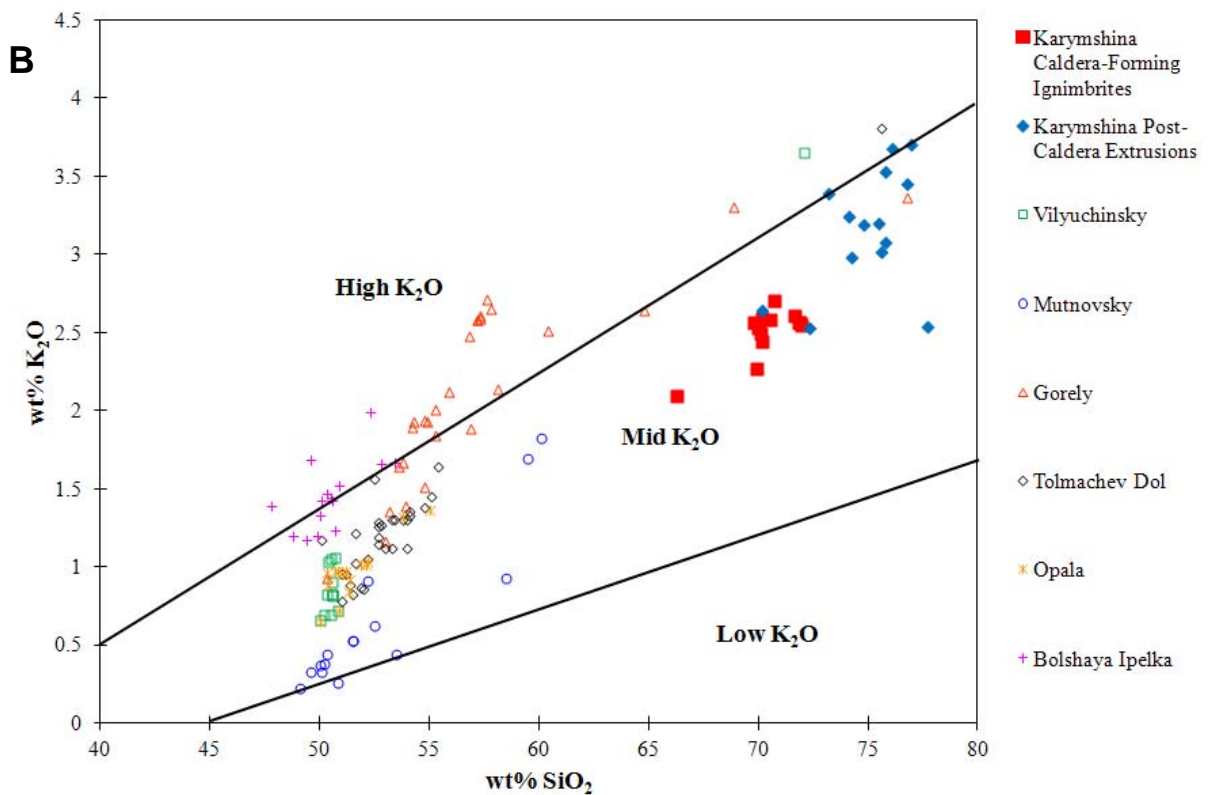
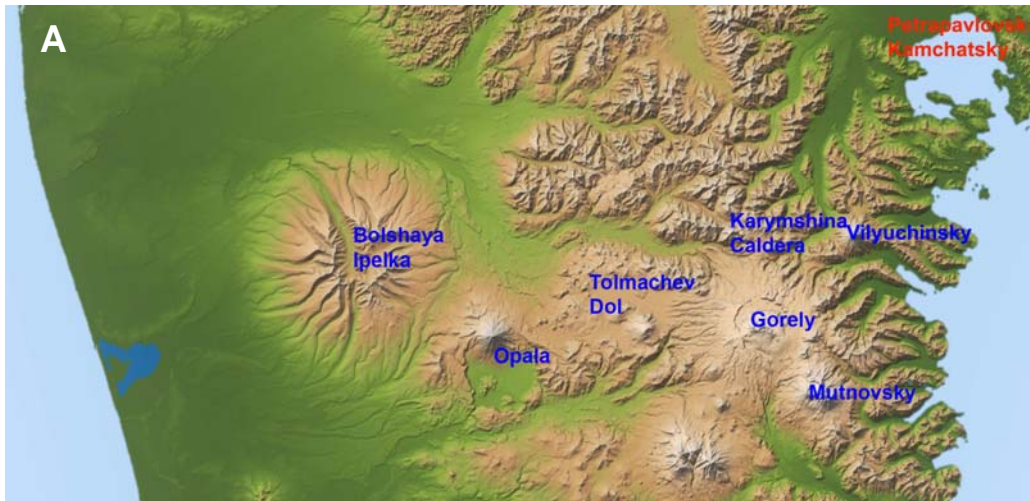


**Figure 10:** A) Map of the Kamchatka Peninsula showing the location of volcanic centers compared in a cross-section from fore-arc to back-arc. B) Graph comparing Karymshina Caldera to other calderas located in a cross-section of the Kamchatka Peninsula, moving away from the subduction zone trench. Data not related to Karymshina Caldera was taken from Portnyagin & Bindeman, unpublished. Karymshina Caldera has much higher  $\text{SiO}_2$  content than the majority of the surrounding volcanic rocks, but has  $\text{K}_2\text{O}$  content that would indicate magmas at Karymshina Caldera were evolved through fractional crystallization or partial melting of the same source material that formed the other rocks.

Sheimovich and Golovin, 2003; Leonov and Rogozin, 2007; Bindeman et al., 2010).

Thus there appear to be two major eruptive periods, approximately 1 million years apart.

The large time period between eruptions and the duration of the second eruptive period may indicate the presence of a crystalline mush from which the magma for both eruptions may have been supplied. This would also account for the apparent evolution of the magma from the ignimbrites to the extrusions (Fig. 7, 10). Such a mush could remain semi-molten within the earth's crust for long time periods while crystallizing and extracting melt (Bachmann & Bergantz, 2004). Based on the hot springs and other volcanic activity near Karymshina Caldera it is quite probable that there is still an active magma chamber beneath Karymshina Caldera, another support for the existence of a crystalline mush in the area.

In addition to Ar-Ar dating, U-Pb dating of zircon crystals from the ignimbrites has been used to determine the crystallization age of the magma. The crystallization age is  $1.87 \pm 0.11$  Ma (Bindeman et al., 2010). This age is identical within error to the eruption age, indicating that crystallization occurred either simultaneously with, or immediately prior to the eruption. This indicates that there was a short zircon residence time prior to the initial, caldera-forming eruption. Zircons in selected post-caldera extrusions, near Babii Kamen, also show no evidence of inheritance (Bindeman et al., 2010), indicating that the age of these zircons is also the crystallization age of the magma.

## *Mineralogy from Thin Sections*

### *Ignimbrites*

The ignimbrites examined in thin section and analyzed with the electron-microprobe have 42-48% glass matrix by volume. Flow textures are visible within the glass matrix and there appears to be no alteration, except in the case of 2005G-5, which contains extensive radial textures indicating post-eruptive alteration of the sample.

The samples contain 16-21% quartz by volume, except in the case of 2005G-5 where only 2% quartz by volume is present. In the majority of samples, the quartz consists of both larger and smaller phenocryst sizes with the larger phenocrysts containing several melt inclusions. In a few quartz phenocrysts the inclusions were so abundant that the quartz appeared skeletal. The larger phenocrysts also exhibit extensive microfracturing, evidence of an explosive eruption (Best and Christiansen, 1997; Bindeman, 2005). In sample 2005G-5, quartz phenocrysts are small and contain no visible melt inclusions.

The other major phase present is plagioclase, which ranges from 19-23% by volume in most of the samples and is 46% by volume of 2005G-5. Many of the larger phenocrysts are made of multiple intergrown crystals (Fig. 11e). The larger phenocrysts also commonly contain melt inclusions and inclusions of other minerals which are too small to identify under the petrographic microscope. While not visible in the smaller phenocrysts, zoning patterns in the larger phenocrysts exhibit a wide range from concentric to extremely complex (Fig. 11). In a few phenocrysts, zoning is not visible at all. Phenocrysts with both core – rim and rim – core extinction are present. Microfracturing in plagioclase phenocrysts is also present, though not as pronounced as in the quartz phenocrysts.

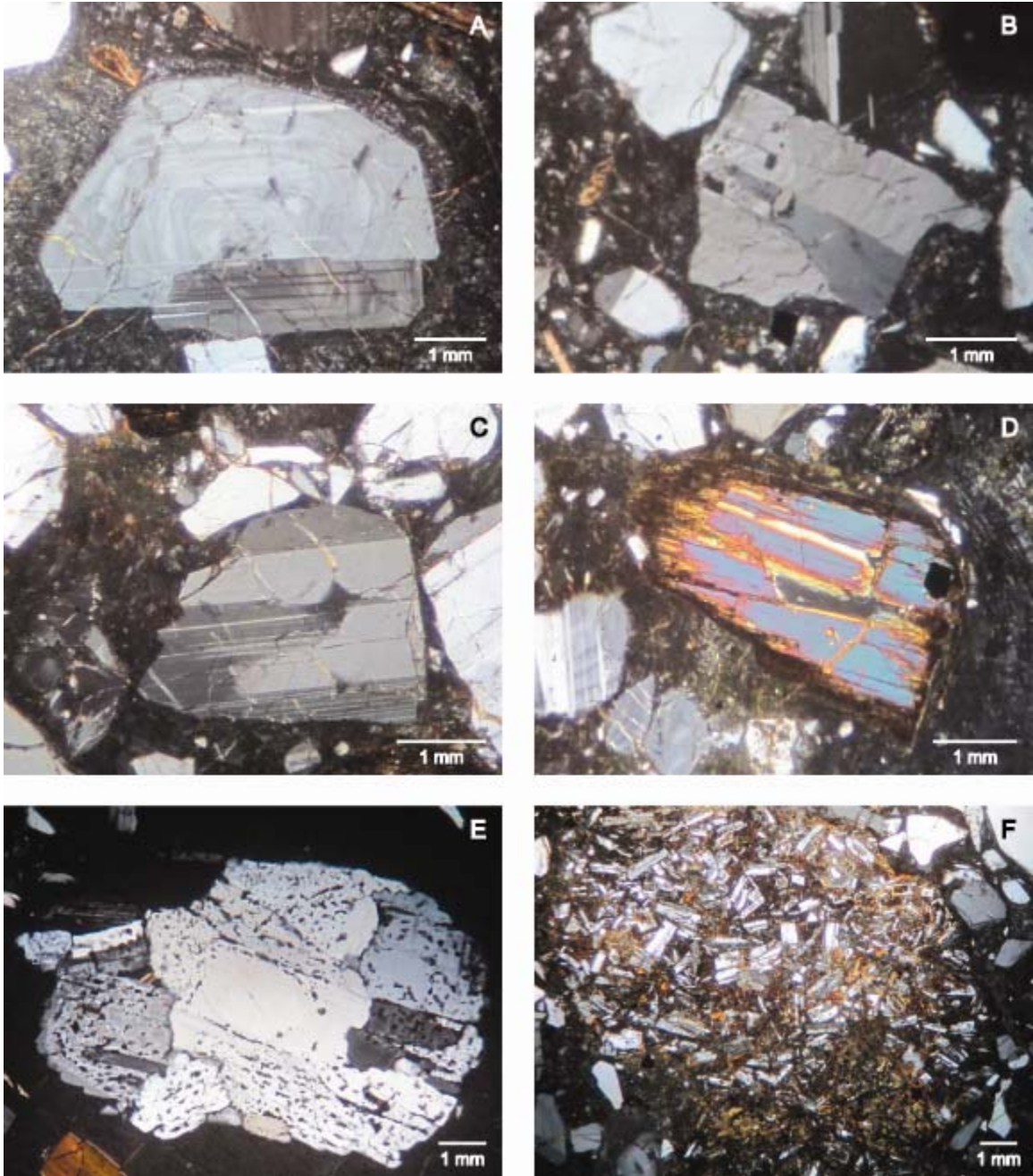


**Figure 11:** Images of various phenocrysts and xenocrysts from thin section samples of Karymshina Caldera. Plagioclase phenocrysts exhibit a) concentric zoning, b) complex zoning, and c) no zoning. Other features present in the Karymshina samples are d) amphibole phenocrysts with reaction rims, e) conglomerations of plagioclase crystals, some with sieve texture, and f) xenoliths which include small phenocrysts of plagioclase.



Biotite in the ignimbrites ranges from 2-12 vol%, with 2005G-5 having the lowest concentration. Many of the biotite crystals have reaction rims, either due to reactions within the magma during crystallization or as a result of alteration after eruption. The results of  $\delta D$  isotope analysis, discussed in more detail below, indicate that the reactions most likely occurred during crystallization. The composition of the reaction rims is not identifiable under the microscope.

The ignimbrites also contain up to 5 vol% amphibole. All amphibole phenocrysts contain reaction rims (Fig. 11d). Compositional analysis of these rims using the electron-microprobe is inconclusive as a mineral formula could not be calculated (Table 2). These rims could be the result of reactions within the magma during crystallization and eruption, or a result of post-eruption alteration. Again, results of  $\delta D$  isotope analysis indicate that the reactions most likely occurred during crystallization. Microfracturing is present in all amphibole phenocrysts, as expected in an explosive eruption.

The remaining material consists of 1-3 vol% opaque minerals and fractures in the rocks filled with microcrystalline quartz in two cases. The opaque minerals are primarily magnetite or hematite, although microprobe analysis shows the presence of trace amounts of ilmenite as well. The hematite is likely a product of post-eruption alteration.

Two of the ignimbrite thin sections (40L-2007 and 36L-2007) contain small xenoliths (Fig. 11f). The xenoliths contain 47-57 vol% glassy matrix and 43-49 vol% plagioclase crystals. The small size of the plagioclase crystals indicates that the magma from which the xenoliths were created cooled quickly. The plagioclase crystals do not have visible zoning, but this is most likely due to the small crystal size which makes all features of the crystals difficult to see. Analysis of the plagioclase crystals in the

xenoliths shows them to be 38.19 wt% albite and 60.50 wt% anorthite, which may indicate that the xenoliths are from early crystallization of the magma. This may have occurred along the walls of the magma chamber where the magma came in contact with cooler crustal material, thus initiating fast cooling of the magma. The rest of the xenoliths are made of 0-4 vol% quartz, 0-3 vol% biotite, and 0-3 vol% opaque minerals (which are most likely magnetite).

### *Post-Caldera Extrusions*

The post-caldera extrusions examined in thin section and analyzed using the electron-microprobe are slightly more evolved in composition, but contain fewer phenocrysts than the ignimbrites. Glassy matrix in these samples ranged from 53-54 vol%. In one of these thin sections perlitic textures are present in the glass matrix, indicating weathering occurred post-eruption.

Quartz ranges from 14-17 vol% in these samples. Larger phenocrysts contain several melt inclusions, in many cases to the point where they border on a sieve texture. The phenocrysts also contain extensive microfracturing, indicating a more explosive eruption despite being from eruptions that built the edifice rather than a caldera-forming eruption.

Plagioclase composes 22-24 vol% of the post-caldera extrusions. As with the ignimbrites, phenocrysts are commonly found as intergrown groups rather than individual crystals. Melt inclusions are common in the larger phenocrysts, creating a sieve texture in many of the phenocrysts. The larger phenocrysts exhibit a range of zoning from

concentric to extremely complex. Both core – rim and rim – core extinction patterns are present. The larger phenocrysts also contain microfractures.

The post-caldera extrusions also contain 4-6 vol% biotite, which appears to be unaltered and would indicate that where perlitic texture is present it is indicative of only early stages of weathering. There are also opaque minerals present (2-3 vol%) which are primarily magnetite with some ilmenite. No xenoliths are present in the post-caldera extrusions.

### *Isotope Analysis*

#### *Oxygen Isotopes ( $\delta^{18}O$ )*

Values of  $\delta^{18}O$  in plagioclase phenocrysts range from 5.71-6.53 ‰ in the caldera-forming ignimbrites and slightly higher at 6.22-6.56 ‰ for the post-caldera extrusions (Table 4). As is typical, the quartz phenocryst values are roughly 1-2.5 ‰ higher, ranging from 7.26-8.12 ‰ and 7.08-7.56 ‰ for the ignimbrites and post-caldera extrusions respectively (Table 4). These values were used to calculate the  $\delta^{18}O$  values for the magma using the equations

$$\delta^{18}O_{\text{qz}} - 0.45 = \delta^{18}O_{\text{magma}} \quad (1)$$

$$0.027(\text{wt\% SiO}_2) - 1.45 + \delta^{18}O_{\text{plag}} = \delta^{18}O_{\text{magma}} \quad (2)$$

for calculation from quartz and plagioclase values, respectively, with equation 1 being based on measurements in the Bishop Tuff (Bindeman & Valley, 2002) and equation 2 based on calculations by Bindeman et al., (2004) and the wt% SiO<sub>2</sub> in equation 2 being that for the whole rock (Bindeman et al., 2004). Where both phases were available, the calculated  $\delta^{18}O_{\text{magma}}$  values were averaged to obtain a best estimate of the  $\delta^{18}O_{\text{magma}}$

value. The resulting  $\delta^{18}\text{O}_{\text{magma}}$  values range from 6.17-7.49 ‰ in the ignimbrites and 6.63-7.10 ‰ for post-caldera extrusions.

These values are higher than for magmas derived by pure fractional crystallization of a MORB source (Fig. 12) (Bindeman, 2008), although the lowest  $\delta^{18}\text{O}_{\text{magma}}$  values for the ignimbrites overlap with pure fractionation trends from MORB source magmas (Fig. 12). It is therefore necessary to incorporate some amount of crustal rock into the magma to obtain the observed range of  $\delta^{18}\text{O}_{\text{magma}}$  values, which supports the results of the rhyolite-MELTS experiments discussed below in this paper. Thus the data from  $\delta^{18}\text{O}$  in this study indicates that the HSR of Karymshina Caldera were likely formed by a similar method to other rhyolitic rocks.

Analyses of zircon phenocrysts show  $\delta^{18}\text{O}$  values ranging on the low side of normal (Table 4). These lower values indicate that a small amount of hydrothermally altered source rock may have been incorporated into the magma, which is likely given the current hydrothermal activity in the area. A hydrothermally-altered assimilant, which would have lower than normal  $\delta^{18}\text{O}$  values, would have been particularly likely if the basaltic parent magma had higher than normal  $\delta^{18}\text{O}$  values, thus creating a magma with normal  $\delta^{18}\text{O}$  values. Recent analysis by Bindeman (unpublished) of a potential pre-caldera basaltic parent rock show higher than normal  $\delta^{18}\text{O}$  values ranging from 5.35-7.48 ‰ in plagioclase phenocrysts from the pre-caldera basalt, indicating that a high- $\delta^{18}\text{O}$  parent magma is possible.

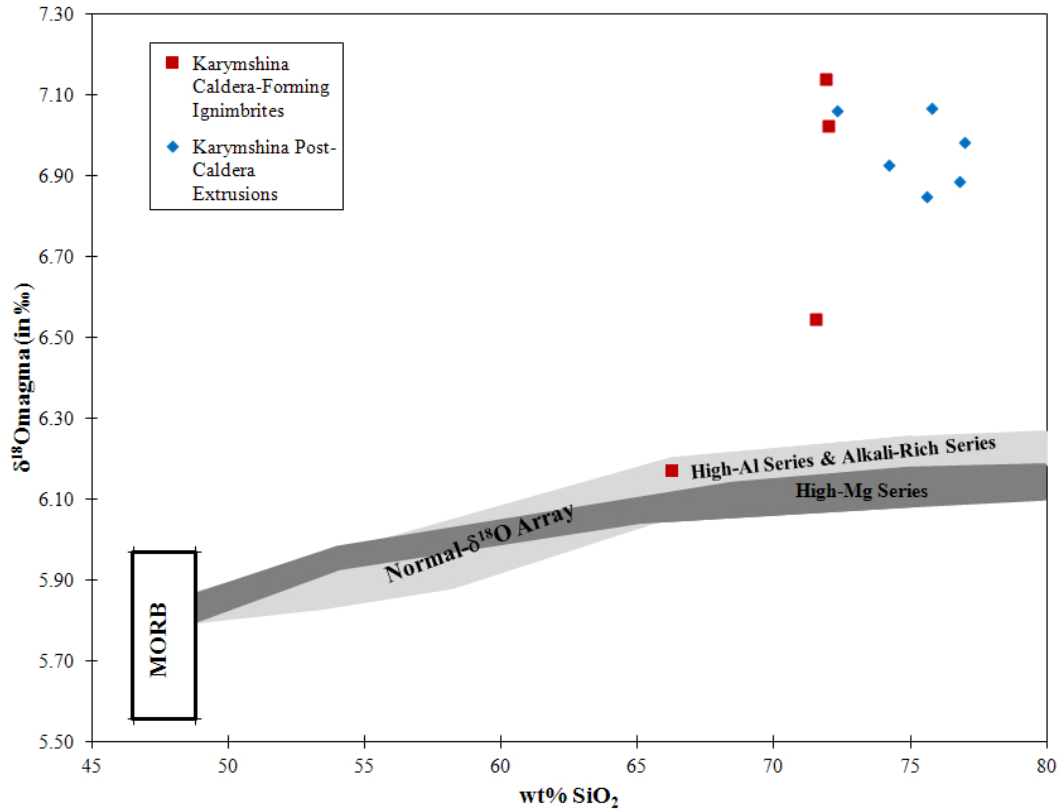


**Figure 12:** The results of crystallization experiments for the three most common island arc series (Normal- $\delta^{18}\text{O}$ ) with a comparison to the Karymshina Caldera samples. The Karymshina samples are located primarily in the area of higher  $\delta^{18}\text{O}$  than would be achieved by fractional crystallization and therefore requires the addition of crustal material containing a higher  $\delta^{18}\text{O}$ . Figure adapted from Bindeman, 2008.

### *Hydrogen Isotopes ( $\delta\text{D}$ )*

Hydrogen isotope values were only obtained for amphibole and biotite-bearing samples of caldera-forming ignimbrite because samples from the extrusions are either too altered or lack amphibole and biotite. Values of  $\delta\text{D}$  range from -109.85 - -142.76 ‰ in biotites and -120.96 ‰ and -148.89 ‰ in the two amphibole samples (44L-2007 and 47L-2007 respectively) (Table 4), which is lower than normal for volcanic rocks in arc environments (Sheppard et al., 1986).

The  $\delta D$  values obtained for both the biotites and the amphiboles are more depleted in D than samples of other volcanic rocks from the EVF of Kamchatka (Fig. 13) studied by Taran et al., 1997, and are some of the lowest measured  $\delta D$  values in Kamchatka. However, the  $H_2O$  contents in both the Karymshina samples and those from other volcanoes are similar and appropriate for fresh amphiboles and biotites.

When compared with the normal rhyolitic  $\delta^{18}O$  values obtained from quartz and plagioclase phenocrysts, the low  $\delta D$  values could be due to post-eruption alteration of the rocks, despite the care taken to avoid altered samples in the selection process, or the low  $\delta D$  values are attributable to hydrothermal alteration of the magma source rock. Such hydrothermal alteration of the source rock would require that a shallow crustal source was assimilated into the magma and therefore would indicate the presence of a shallow magma chamber.

#### *$^{87}Sr/^{86}Sr$ Isotope Ratios*

Ratios of  $^{87}Sr/^{86}Sr$  were determined for whole rock samples of caldera-forming ignimbrites. Values range from 0.703317 – 0.703328 (Table 4), which is indicative of a predominance of mantle-derived material within the magma (Fig. 14) (Faure & Mensing, 2005). It is possible that assimilated crustal rocks in Kamchatka, even with hydrothermal alteration, could have a relatively low  $^{87}Sr/^{86}Sr$  ratio (e.g. Bindeman et al., 2004) since the area is a subduction zone and the majority of rocks in the peninsula originated through subduction processes. However, by using values from Bindeman et al. (2004) for crustal and mantle sources in Kamchatka, it is apparent that the primary magma source at Karymshina Caldera must have originated in the mantle (Fig. 14). Some crustal

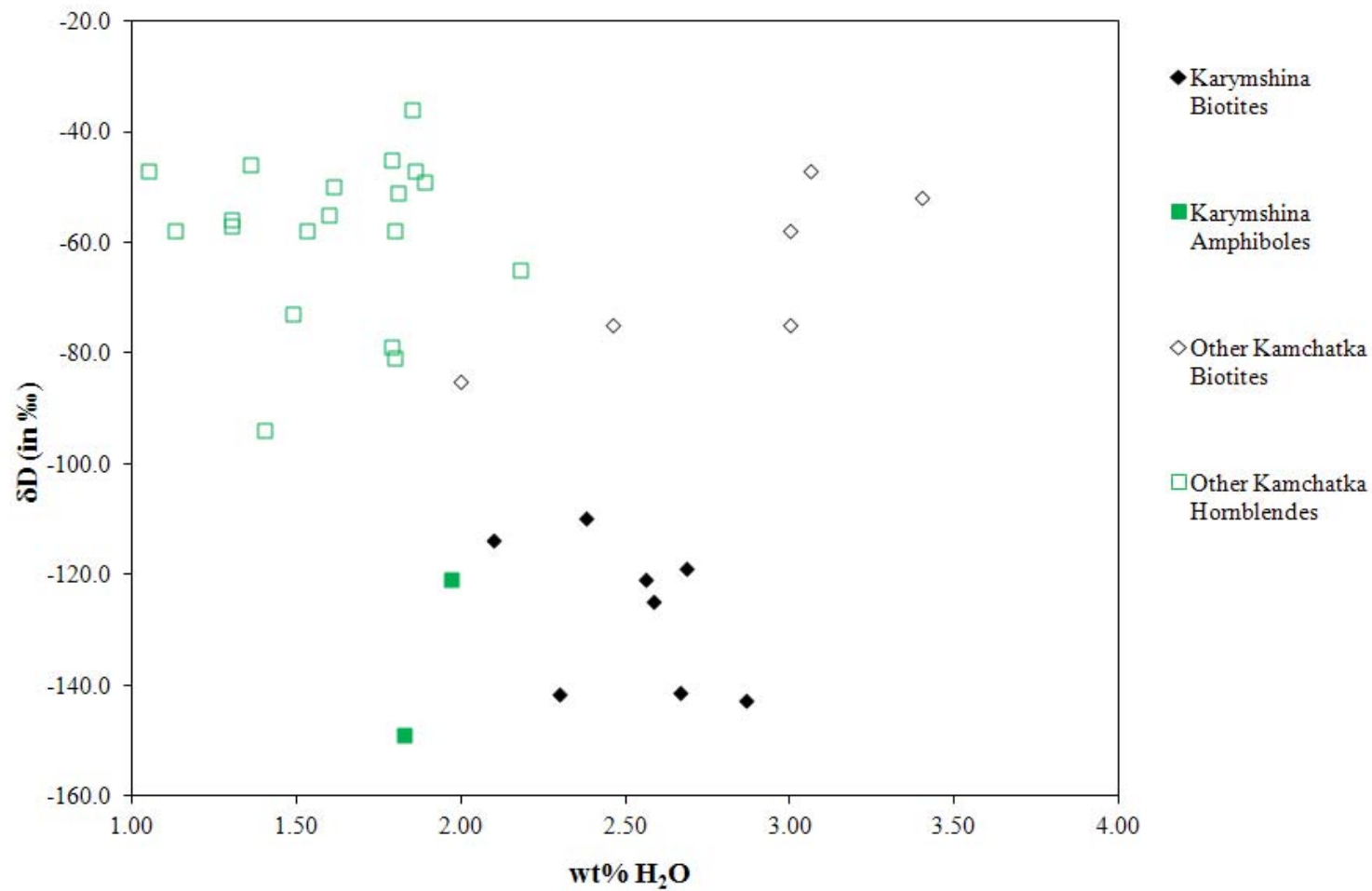


**Figure 13:** A graph comparing  $\delta D$  values vs. wt% H<sub>2</sub>O for biotites and amphiboles from caldera-forming ignimbrites at Karymshina Caldera to other samples from the Eastern Volcanic Front. The data for the additional samples was taken from Taran et al., (1997).

values within the EVF are even closer to mantle values than the values used here (Bindeman et al., 2004) and thus it may be impossible to determine whether the Karymshina Caldera magma came from primarily a crustal or mantle source.

#### *<sup>144</sup>Nd/<sup>143</sup>Nd Isotope Ratios*

Caldera-forming ignimbrites were also analyzed for <sup>144</sup>Nd/<sup>143</sup>Nd ratios. The resulting values range from 0.513015 – 0.513065 (Table 4). These values indicate a primarily mantle source for the magma (Fig. 14) (Faure & Mensing, 2005), in agreement with the <sup>87</sup>Sr/<sup>86</sup>Sr values. Therefore, either the crustal source rocks have lower <sup>87</sup>Sr/<sup>86</sup>Sr and higher <sup>144</sup>Nd/<sup>143</sup>Nd than normal for crustal rocks or the majority of the magma (at least 90% by weight) is from a mantle source (Bindeman et al., 2004; Faure & Mensing, 2005).



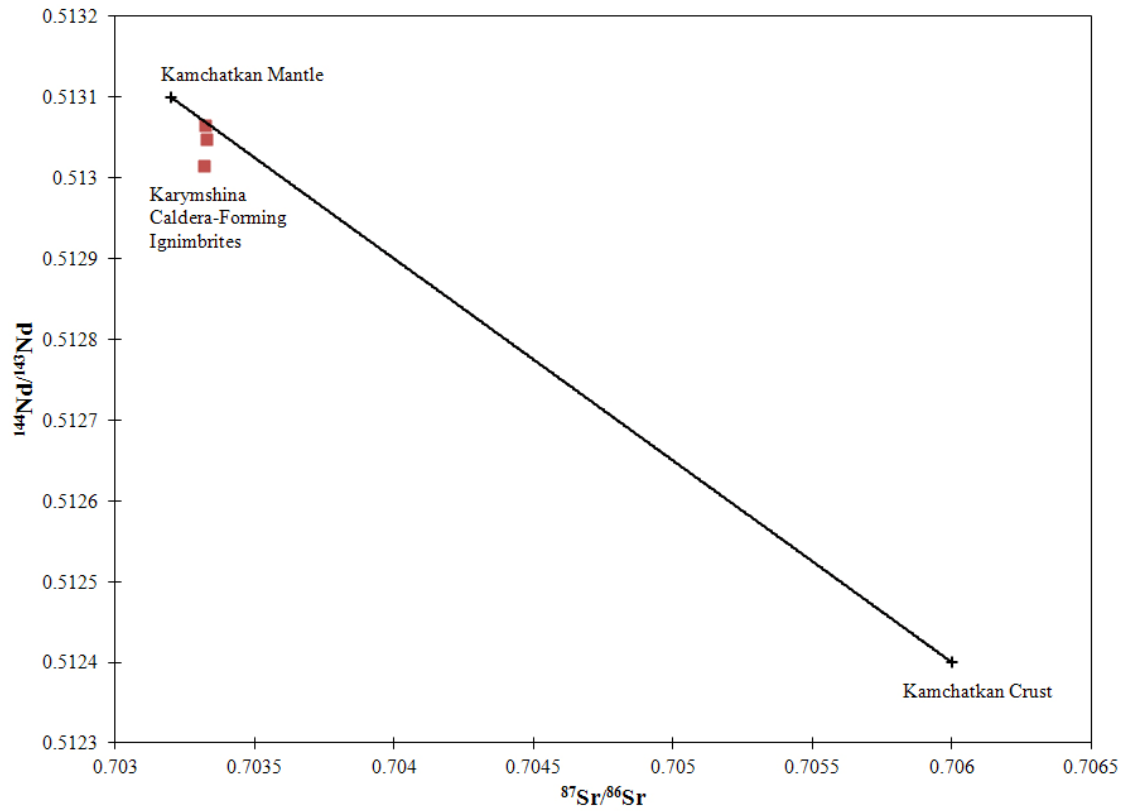


**Figure 14:** An approximate mixing trend for  $^{87}\text{Sr}/^{86}\text{Sr}$  and  $^{144}\text{Nd}/^{143}\text{Nd}$  with an average crustal and mantle magma from the Kamchatka Peninsula as compared to caldera-forming ignimbrites from Karymshina Caldera. The crustal and mantle values were taken from Bindeman et al., 2004.

## CHAPTER V

### MELTS MODELING

#### *Methods*

To elucidate the origin of the Karymshina ignimbrites, I conducted crystallization and assimilation modeling experiments using the rhyolite-MELTS program developed by Gualda et al. (2011). The initial composition of basaltic magma was selected from data for volcanoes surrounding Karymshina Caldera. Several samples were compared (Fig. 15) and the composition most closely resembling a primitive magma from which the Karymshina magmas may have been derived was selected (the Gorely composition from Portnyagin and Bindeman (unpublished) (Table 5)). The assimilant composition used was an amphibolite partial melt taken from the experiments of Rapp and Watson (1995), which is referred to below as APM. This composition was chosen because there are no actual partial melting experiments that have been done on rocks found near Karymshina Caldera, but amphibolite is a common metamorphic rock on the Kamchatka Peninsula (Kepezhinskas et al., 1997) and is a common composition for the lower crust of continents (Rapp and Watson, 1995; Annen and Sparks, 2002). It is therefore likely that partial melts of an amphibolite source would be assimilated into the magma chamber at Karymshina Caldera. A hydrothermally-altered rock, IC50, with SiO<sub>2</sub> contents of 81.34 wt% obtained from Bindeman (unpublished) (referred to below as HAR) was also used as an assimilant as this type of rock may also have been added to the magma if remelting and recycling occurred in the magma generation process.

Fractional crystallization was modeled with 0 and 2.5 wt% H<sub>2</sub>O in the initial basalt and 0, 25, and 50 wt% APM and 0 and 10 wt% HAR. These models were

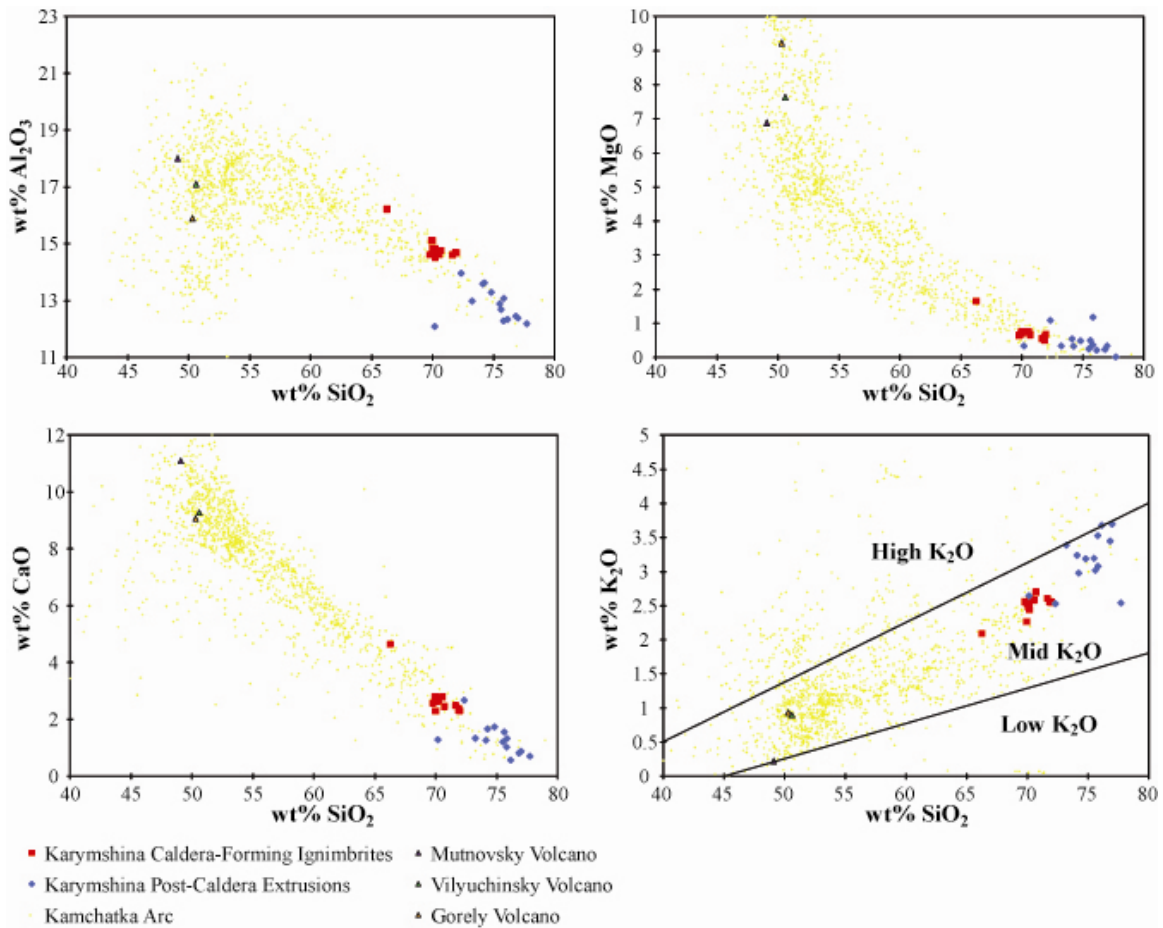


**Figure 15:** Graphs for selected compositional variables comparing the three possible starting compositions for use in rhyolite-MELTS modeling. The three starting compositions were taken from Portnyagin and Bindeman, unpublished.

conducted at 2 kbar, 8 kbar, and also a polybaric model starting at 8 kbar and moving to 2 kbar at 50 wt% crystallization. One set of models using only the initial basalt compositions were conducted with equilibrium crystallization (Fig. 16) to verify that the compositions seen at Karymshina Caldera could not have been the result of equilibrium crystallization. All other models were conducted using fractional crystallization. In the case of the polybaric models, change in pressure was assumed to be instantaneous based on probable speed of magma ascent from Annen et al. (2006).

**Table 5:** Compositions of the starting magma and assimilants used in the rhyolite-MELTS models. The starting magma (Gorely Volcano N69) was taken from Portnyagin & Bindeman, (unpublished), the amphibolite partial melt was taken from Rapp & Watson, (1995), and the hydrothermally-altered rock was taken from Bindeman, (unpublished).

<b>Sample Number</b>	<b>Gorely Volcano N69</b>	<b>Partial Melt of JOD-74 at 8 kbar and 1000°C</b>	<b>Hydrothermally Altered Rock IC50</b>
SiO <sub>2</sub>	50.3	71.14	81.34
TiO <sub>2</sub>	1.05	0.18	0.188
Al <sub>2</sub> O <sub>3</sub>	15.9	17.67	12.45
FeO*		2.05	0.95
Fe <sub>2</sub> O <sub>3</sub>	10.2		
MnO	0.17	0.08	0.043
MgO	9.22	0.48	0.27
CaO	9.07	1.24	1.06
Na <sub>2</sub> O	2.9	5.04	2.29
K <sub>2</sub> O	0.93	2.12	1.39
P <sub>2</sub> O <sub>5</sub>	0.29		0.016
H <sub>2</sub> O	0.18		
CO <sub>2</sub>	0.02		
Sum	100.2	100	100

## *Results*

The results for equilibrium crystallization of the basaltic parent magma chosen show that it is impossible to obtain the composition of Karymshina Caldera magma by simple crystallization (Fig. 16). The results of the fractional crystallization models obtained compositions closer to those observed at Karymshina Caldera, and these results are represented in figures 17-22 for selected major elements.

Most of the fractional crystallization models resulted in strong enrichments of K<sub>2</sub>O, the exception being 2.5 wt% H<sub>2</sub>O with 25 wt% APM and 10 wt% HAR. This is most likely due to the initial basalt composition containing more K<sub>2</sub>O than was present in

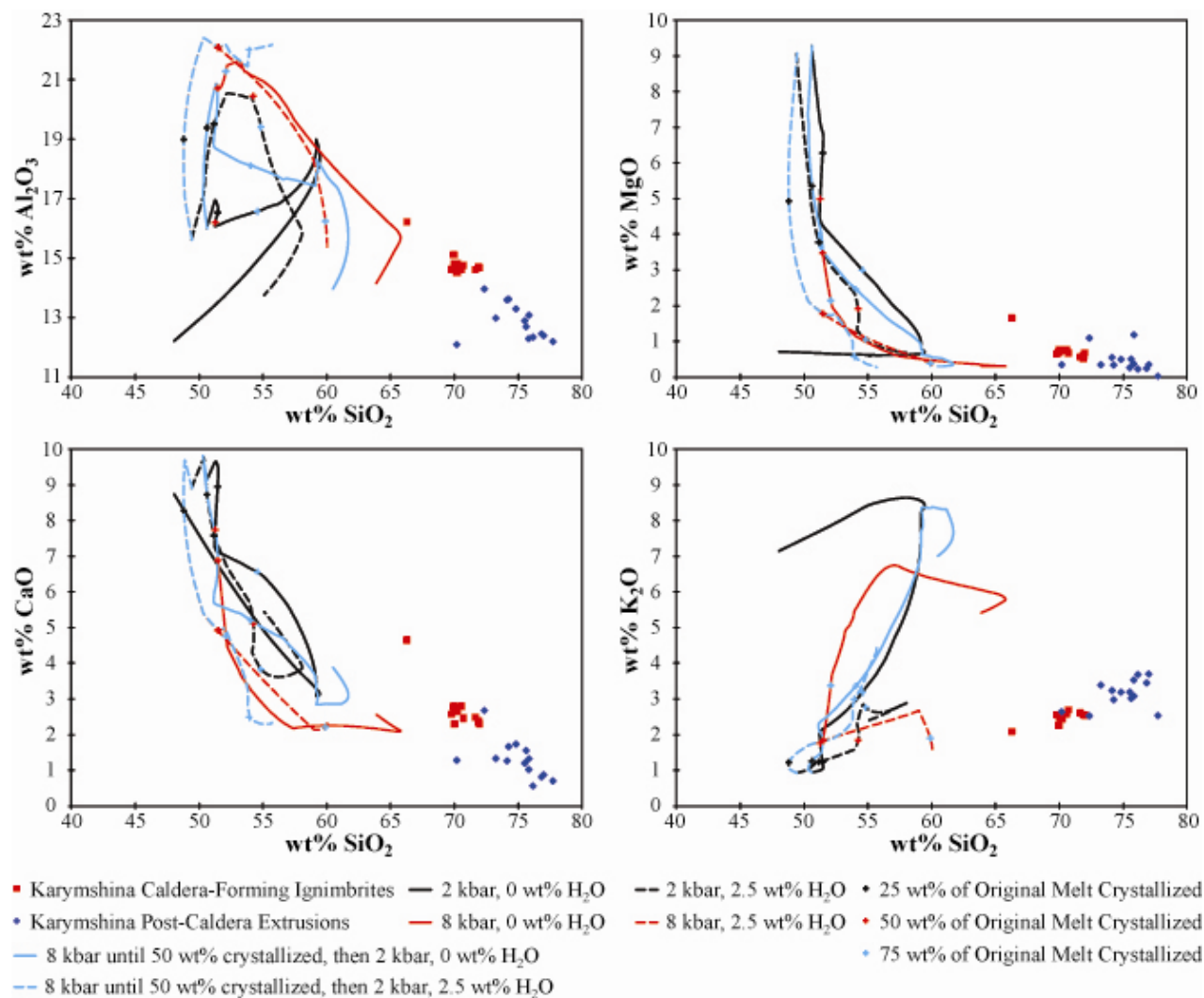


**Figure 16:** Results of equilibrium crystallization modeling at various pressures using the rhyolite-MELTS program. Results are shown for 0 wt% H<sub>2</sub>O and 2.5 wt% H<sub>2</sub>O in the initial melt composition.

the true parent magma of the Karymshina rocks. Fractional crystallization at shallow depths (2 kbar) resulted in the least enrichment of  $K_2O$  as well as a greater increase in the  $SiO_2$  content of the remaining magma (Fig. 17, 18). The models containing 50 wt% APM and 10 wt% HAR were closest to the actual  $K_2O$  and  $SiO_2$  contents of the Karymshina rocks in all cases. In the 2 kbar models, the magma with 2.5 wt%  $H_2O$ , 25 wt% APM, and 10 wt% HAR also matched well with the actual values measured in the Karymshina rocks. In the models with 50 wt% APM,  $SiO_2$  contents equal to those of Karymshina were obtained at all pressure options and approximately when 50 wt% of the magma was crystallized. The models giving the best approximations of fractional crystallization leading to Karymshina rock compositions also match well with a straight line mixing trend between the initial basaltic magma and the Karymshina rocks, indicating that the Karymshina rocks could also be the result of pure magma mixing between some higher  $SiO_2$  magma and a basaltic magma. If this is the case, the Karymshina magmas would likely be primarily composed of amphibolite partial melts and hydrothermally-altered rocks with a small portion (less than 25 wt%) of basaltic magma included. However, this would contradict the data obtained from the isotope analysis.

The results of the fractional crystallization models for the  $Al_2O_3$ ,  $MgO$ , and  $CaO$  were similar to those for  $K_2O$  and  $SiO_2$  contents. The best fits for  $Al_2O_3$  and  $MgO$  occurred with 0 and 2.5 wt%  $H_2O$ , 50 wt% APM, and 10 wt% HAR in the model with pressures starting at 8 kbar and ending at 2 kbar. However, the model at 2 kbar with 2.5wt%  $H_2O$ , 50 wt% APM, and 10 wt% HAR is also a fairly reasonable fit. In terms of

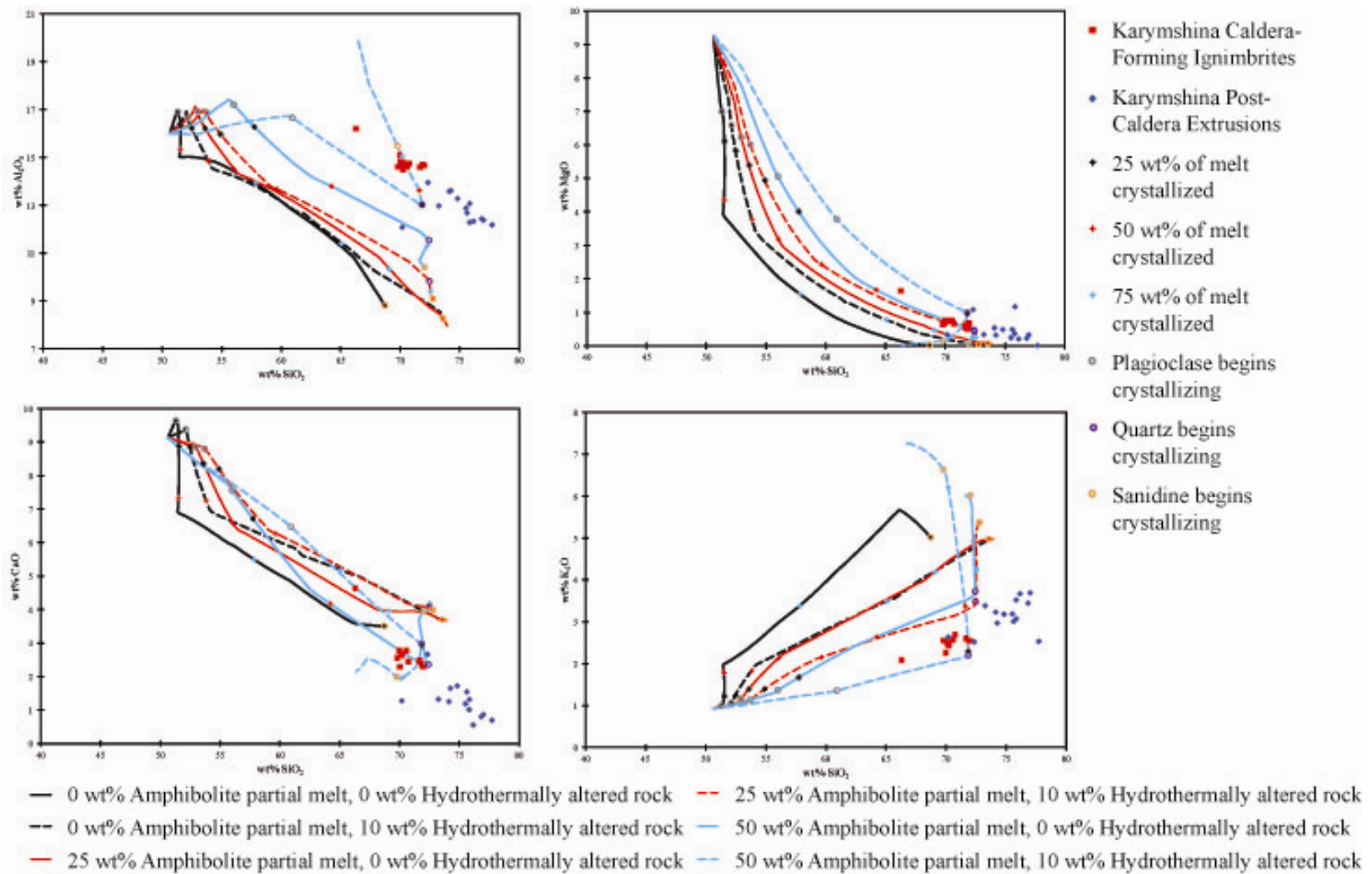


**Figure 17:** Results of fractional crystallization modeling at 2 kbar using the rhyolite-MELTS program. Results are shown for 0 wt% H<sub>2</sub>O in the initial melt composition. The percentages of added amphibolite partial melt and hydrothermally altered melt are as indicated. Amphibolite partial melt and hydrothermally altered melt were added incrementally during crystallization.

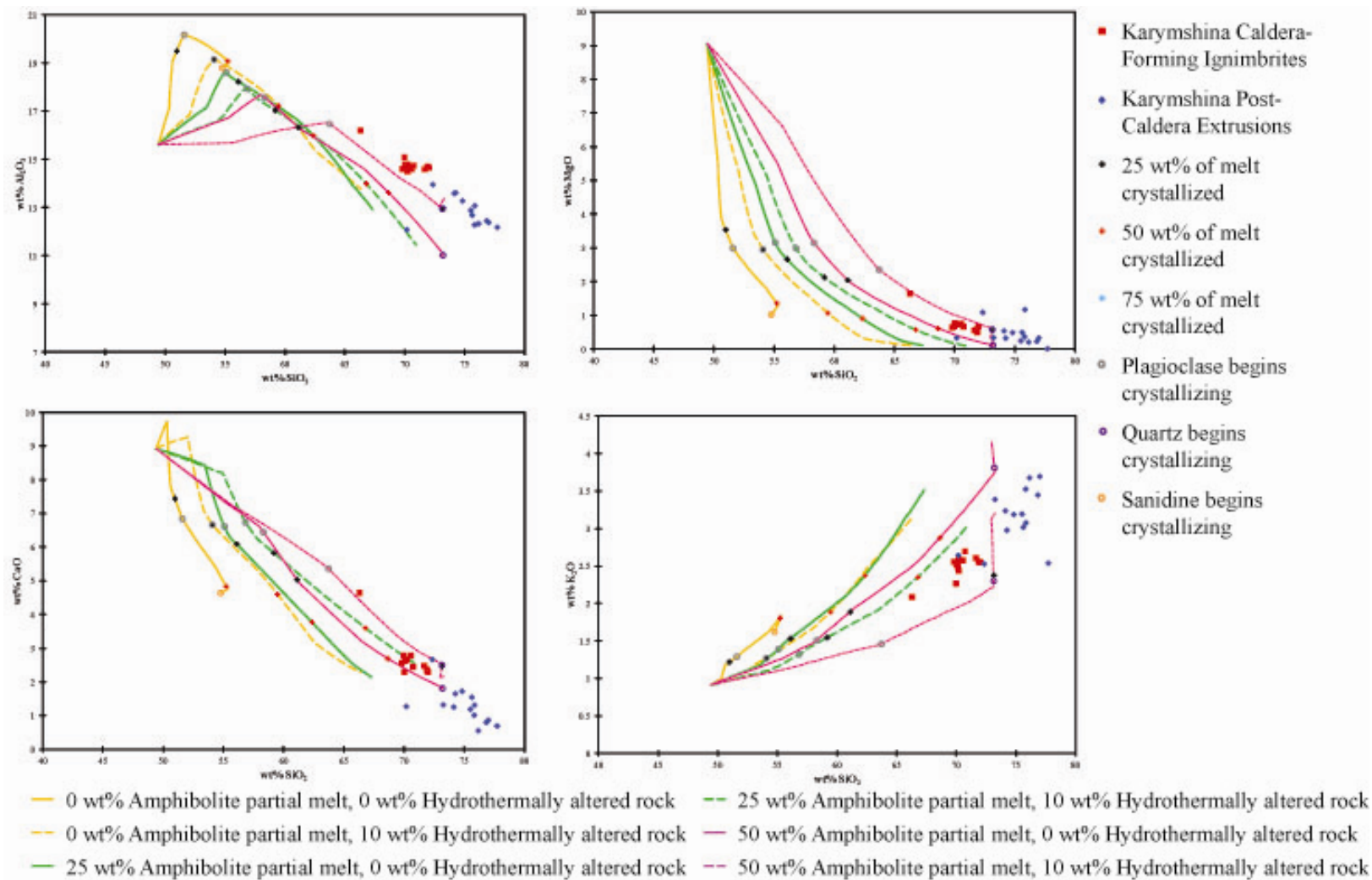


**Figure 18:** Results of fractional crystallization modeling at 2 kbar using the rhyolite-MELTS program. Results are shown for 2.5 wt% H<sub>2</sub>O in the initial melt composition. The percentages of added amphibolite partial melt and hydrothermally altered melt are as indicated. Amphibolite partial melt and hydrothermally altered melt were added incrementally during crystallization.



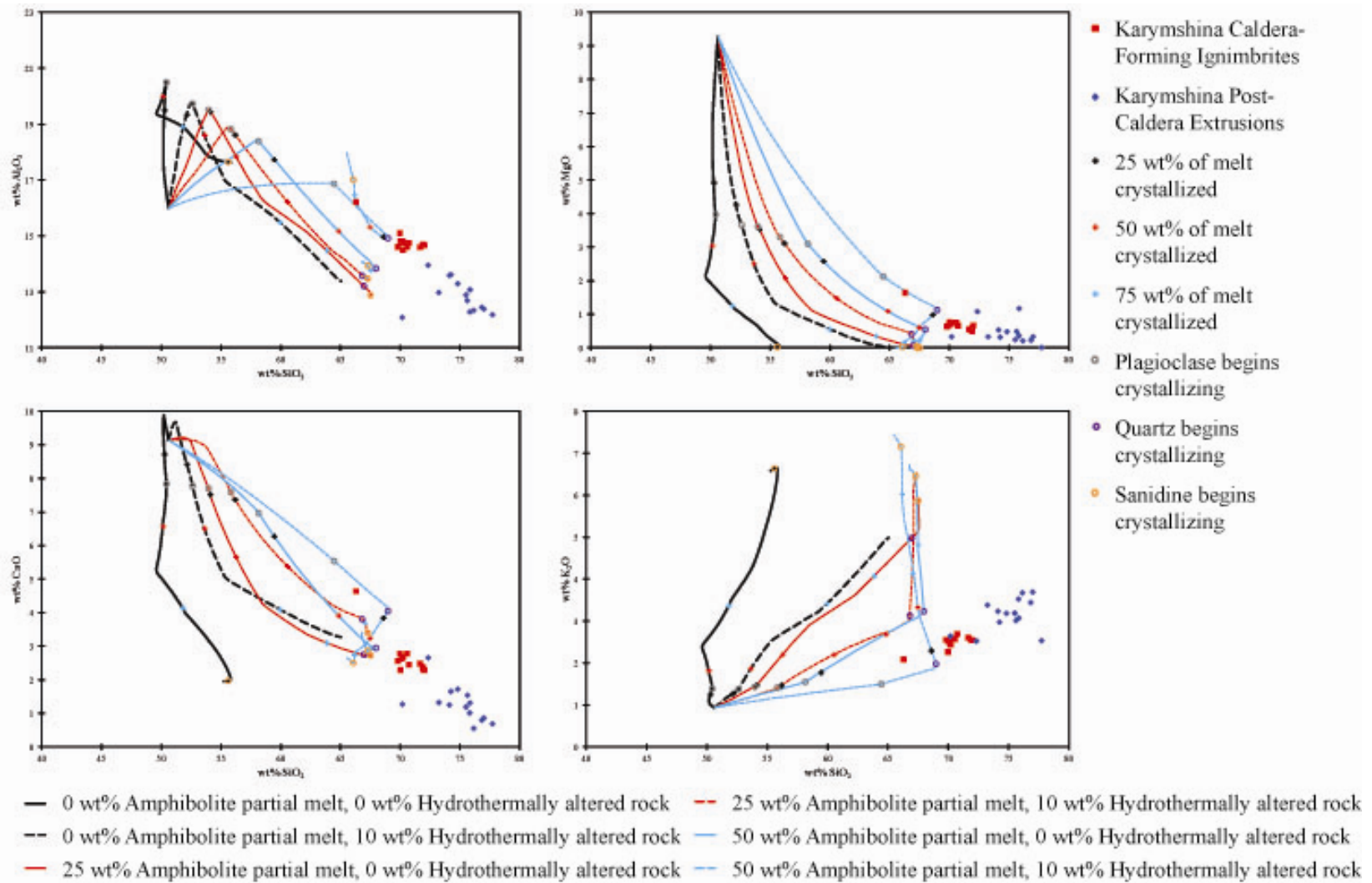


**Figure 19:** Results of fractional crystallization modeling at 8 kbar using the rhyolite-MELTS program. Results are shown for 0 wt% H<sub>2</sub>O in the initial melt composition. The percentages of added amphibolite partial melt and hydrothermally altered melt are as indicated. Amphibolite partial melt and hydrothermally altered melt were added incrementally during crystallization.

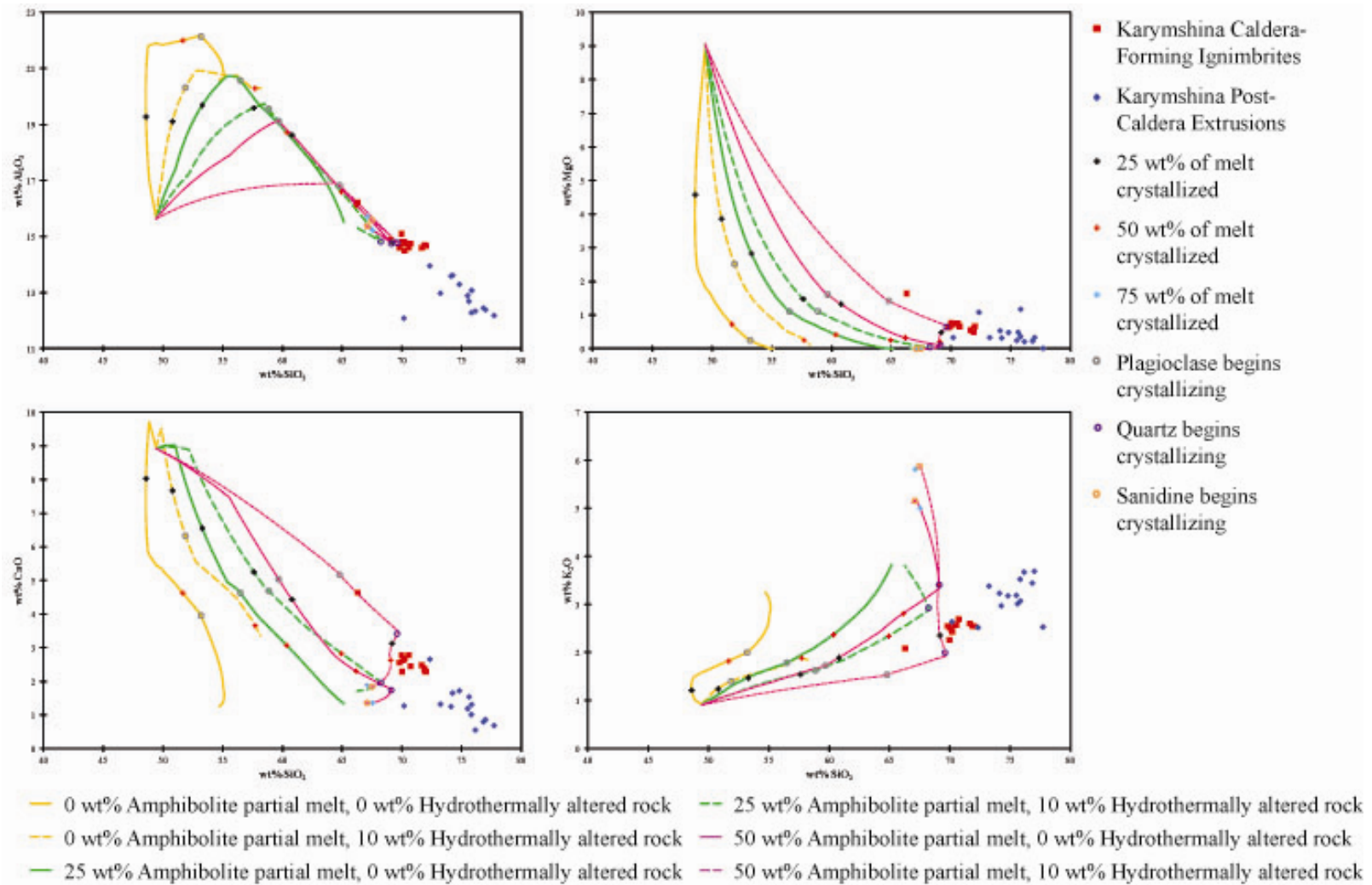


**Figure 20:** Results of fractional crystallization modeling at 8 kbar using the rhyolite-MELTS program. Results are shown for 2.5 wt% H<sub>2</sub>O in the initial melt composition. The percentages of added amphibolite partial melt and hydrothermally altered melt are as indicated. Amphibolite partial melt and hydrothermally altered melt were added incrementally during crystallization.

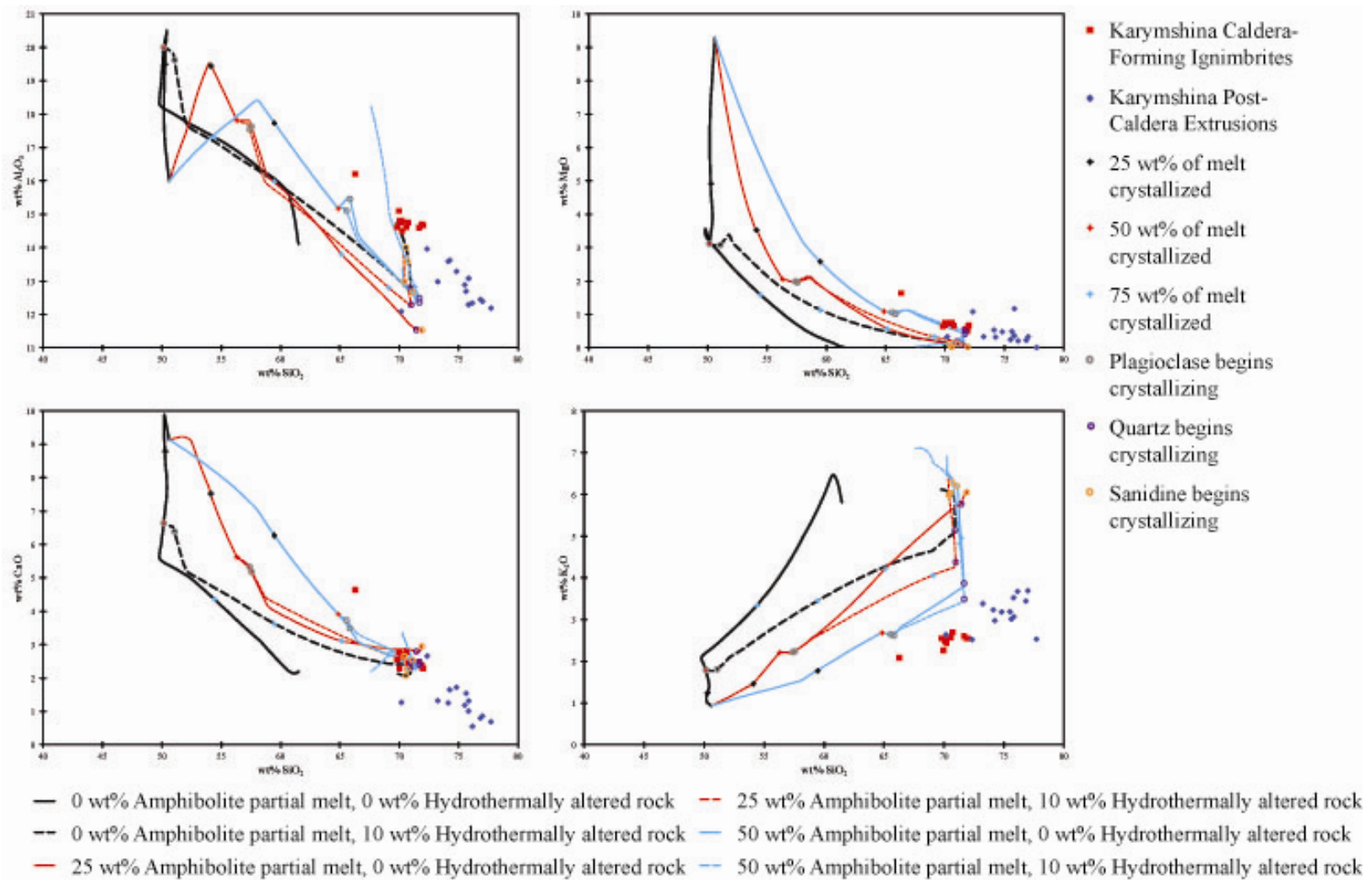


**Figure 21:** Results of fractional crystallization modeling starting at 8 kbar and changing to 2 kbar at 50 wt% crystallization using the rhyolite-MELTS program. Results are shown for 0 wt% H<sub>2</sub>O in the initial melt composition. The percentages of added amphibolite partial melt and hydrothermally altered melt are as indicated. Amphibolite partial melt and hydrothermally altered melt were added incrementally during crystallization.

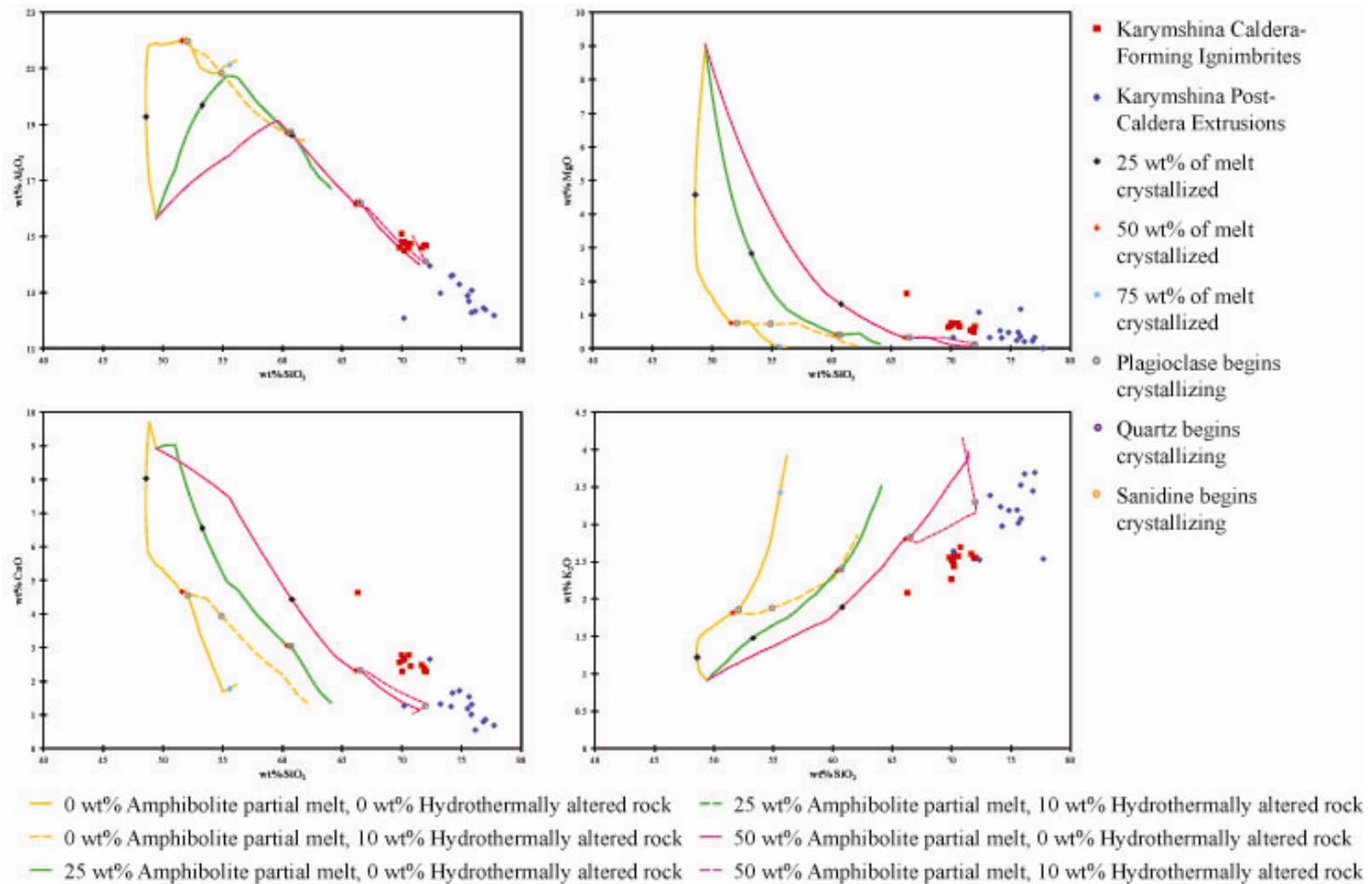


**Figure 22:** Results of fractional crystallization modeling starting at 8 kbar and changing to 2 kbar at 50 wt% crystallization using the rhyolite-MELTS program. Results are shown for 2.5 wt% H<sub>2</sub>O in the initial melt composition. The percentages of added amphibolite partial melt and hydrothermally altered melt are as indicated. Amphibolite partial melt and hydrothermally altered melt were added incrementally during crystallization.

CaO, the models at 2 kbar and 2.5 wt% H<sub>2</sub>O with 50 wt% APM and both 0 and 10 wt% HAR as well as the model with 2.5 wt% H<sub>2</sub>O, 25 wt% APM, and 10 wt% HAR are good fits to the Karymshina rocks. Thus the fractional crystallization model which matched most closely the composition of the Karymshina rocks occurred at 2 kbar with 2.5 wt% H<sub>2</sub>O, 50 wt% APM, and 10 wt% HAR. It should be noted that I was unable to reproduce the most silicic compositions present at Karymshina, represented as post-caldera extrusions. An additional amount of high-silica assimilant like the hydrothermally-altered rock may be required to produce these compositions.

## CHAPTER VI

### DISCUSSION

The Karymshina silicic center is a large-volume caldera that has produced high-silica rhyolitic (HSR) magma. Analyses of the caldera-forming ignimbrites and post-caldera extrusions indicate that  $\delta^{18}\text{O}$  and  $\delta\text{D}$  values of minerals are typical of HSR magmas (Fig. 23) (Bindeman, 2008). However, the  $\delta^{18}\text{O}$  values of the zircons are on the low side of what is normal for rhyolites, allowing the presence of a small amount of hydrothermally altered material incorporated into the magma. High  $\delta^{18}\text{O}$  values (6.1 ‰) recently obtained for pre-caldera basalts and dacites at Karymshina indicate that the  $\delta^{18}\text{O}$  values we should see for the Karymshina Caldera rhyolites would be 0.5 – 1 ‰ higher than what is observed. This further supports the hypothesis of a hydrothermally altered rock with low  $\delta^{18}\text{O}$  values being assimilated into the magma to bring  $\delta^{18}\text{O}$  values into the normal range. The normal  $\delta^{18}\text{O}$  values for quartz and plagioclase and low  $\delta\text{D}$  values combined with a lack of visible alteration in thin section indicate that the low  $\delta^{18}\text{O}$  values in the zircons and low  $\delta\text{D}$  values in amphibole and biotite are more likely due to incorporation of the material into the magma than to post-eruption alteration. The  $^{87}\text{Sr}/^{86}\text{Sr}$  and  $^{144}\text{Nd}/^{143}\text{Nd}$  values obtained initially indicated that a small amount of crustal material was incorporated into the magma. Closer examination shows that these values may be a result of near-mantle values in the crustal rock of the EVF, making the  $^{87}\text{Sr}/^{86}\text{Sr}$  and  $^{144}\text{Nd}/^{143}\text{Nd}$  values irrelevant as indicators of crustal assimilation into the magma (Fig. 14) (Bindeman et al., 2004; Faure & Mensing, 2005).

Modeling using rhyolite-MELTS (Gualda et al., 2011) also indicates that it is necessary to incorporate crustal material into the magma to obtain the proper magma

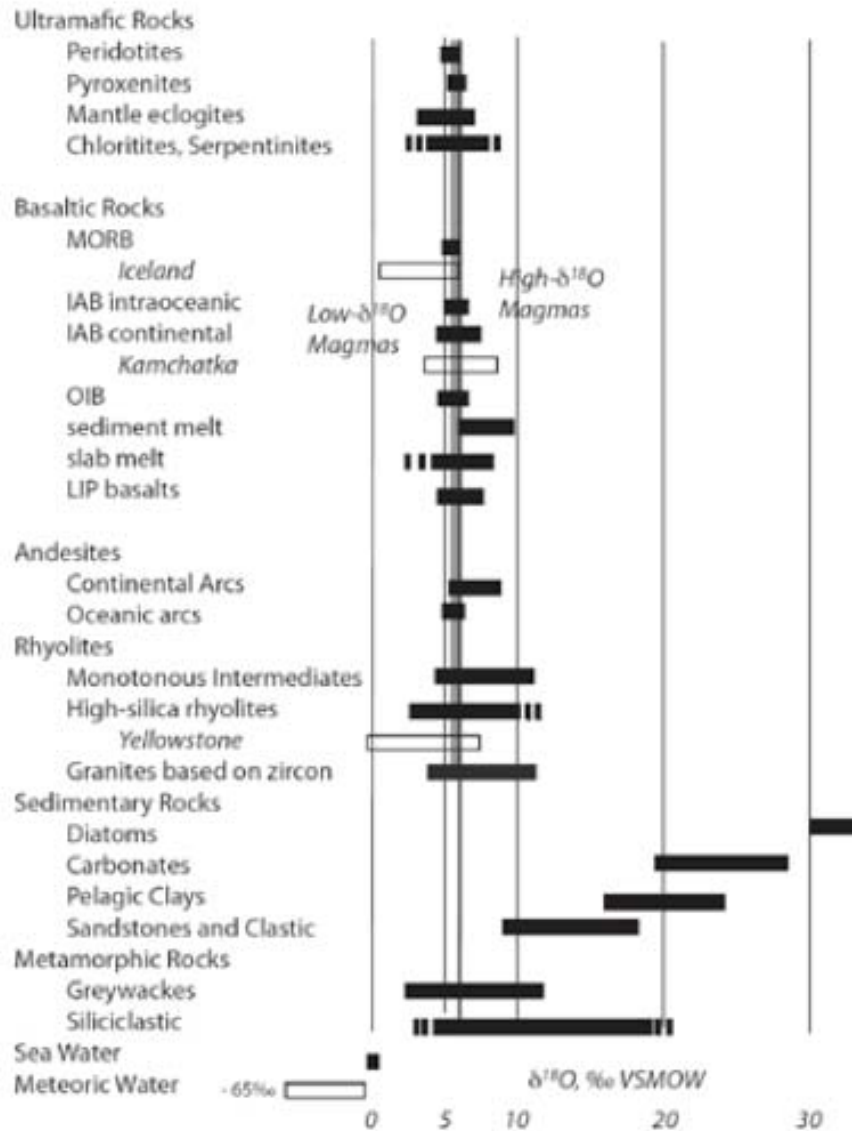


**Figure 23:** A diagram showing the normal values of  $\delta^{18}\text{O}$  in various rock types. Karymshina Caldera falls within the normal range for HSR magmas. The diagram was taken from Bindeman, (2008).

composition, assuming that the starting magma is a good approximation of the initial magma at Karymshina Caldera. However, the amount of crustal component needed in the rhyolite-MELTS models is greater than the initially estimated amount from  $^{87}\text{Sr}/^{86}\text{Sr}$  and  $^{144}\text{Nd}/^{143}\text{Nd}$  values. Based on the isotope values, approximately 10 wt% crustal

material is needed, but based on the rhyolite-MELTS models, the crustal component needs to make up more than 50 wt% of the magma even with more than 75% crystallization of the magma by fractional crystallization processes. This may be a fault of the model used, the initial magma composition chosen, the crustal component chosen, the hydrothermally-altered rock chosen, or any combination of these factors. Alternatively, the Sr and Nd values in the actual crustal component and hydrothermally-altered component may be closer to mantle values, even compared to crustal values in Kamchatka. As isotopic variations in Kamchatka are somewhat limited, especially within the Eastern Volcanic Front (Turner et al., 1998; Bindeman et al., 2004), this hypothesis is justified.

Data for elemental Rb and Sr values put the Karymshina Caldera rocks (Fig. 24) within the I-type granitoids, indicating less differentiation of Rb and Sr (Halliday et al., 1991; Bachmann & Bergantz, 2004). I-type granitoids are common in subduction zones and have Rb and Sr values that are closer to mantle values, indicating the magma is less evolved and has undergone less fractional crystallization than typical granitic magmas. The values for the Karymshina Caldera rocks appear to be typical of subduction zones under continental crust, similar to the Peru Coastal Batholith and the Kosciusko Batholith of the Halliday et al. study. Less differentiation of Rb and Sr requires that there be a larger degree of partial melting or fractional crystallization of the parent magma. When dealing with large amounts of either partial melting or fractional crystallization, the ratio of Rb/Sr tends to vary less and give less indication of which process produced the resultant rock. In either case, it is likely that at least 50 wt% of the parent material must be partially melted or fractionally crystallized to produce the rocks of Karymshina



Caldera. If we assume a greater portion of the magma came from the mantle, then the magma was produced primarily through fractional crystallization. If the greater portion

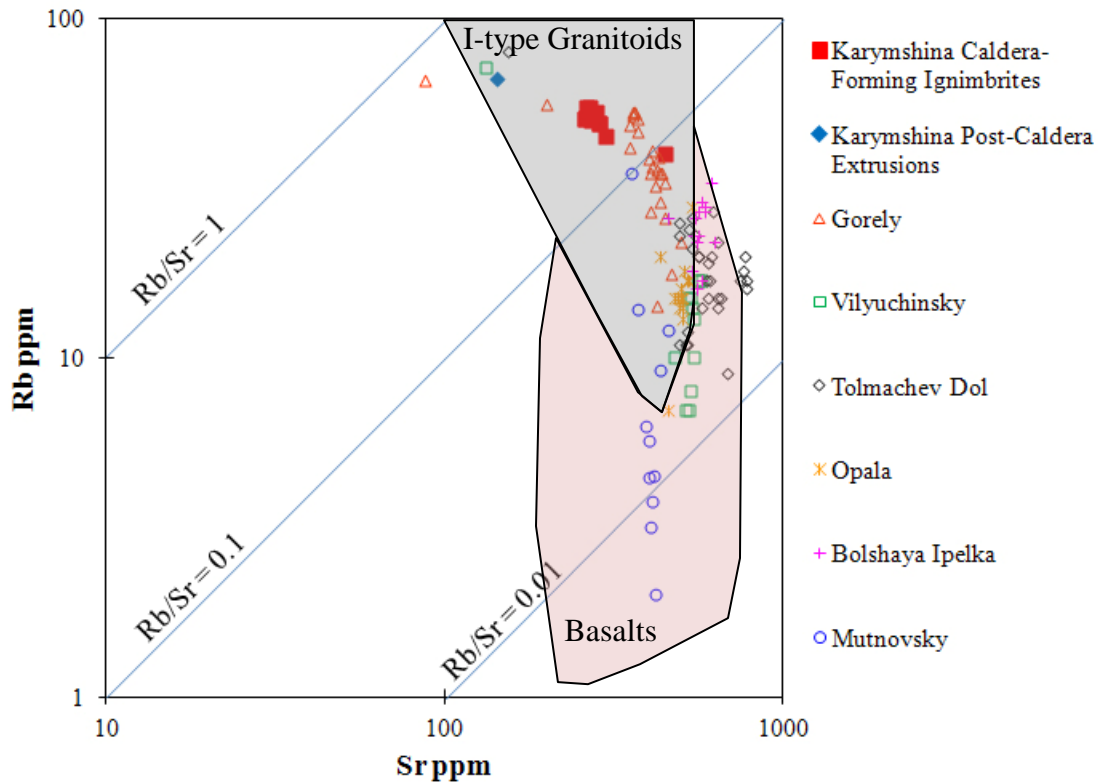


**Figure 24:** Graph of Rb vs. Sr for Karymshina Caldera and a cross-section of the Kamchatka Peninsula. The Karymshina Caldera samples fall within the range of I-type granitoids present in the Halliday et al., (1991) study. Except for a few samples that are higher in Rb and lower in Sr, the other samples fall within the range of basalts and some I-type granitoids. In all the Karymshina Caldera samples, large amounts of fractional crystallization or partial melting would be needed to obtain the observed values. Data for other volcanoes was taken from Portnyagin & Bindeman, (unpublished).

of the magma came from crustal material, then partial melting is the primary method of production.

Of the four main hypotheses for generation of HSR magmas (deep crustal hot zone, crystalline mush, crustal underplating, and upper crustal recycling), it is clear that crustal underplating is definitely not the method by which the HSR magma at

Karymshina Caldera was formed as this would require that the magma be formed from crustal material only. This would contradict the various isotope evidence, which indicates that the crustal component is only a portion of the magma. In addition, it would be difficult to generate such large volumes of magma without incorporating any magma from deeper in the crust due to the amount of heat needed.

It is likely that the Karymshina magma was formed by a combination of the other three methods since the deep crustal hot zone method allows for partial melting of the crust, which would incorporate a crustal component (Annen et al., 2006). This deep crustal hot zone would also provide a constant source of magma recharge and heat to the developing magma chamber located at the shallower depth. The partial melting of the crust would also produce a high-SiO<sub>2</sub> content (Rapp & Watson, 1995) component, which would raise the overall SiO<sub>2</sub> content of the magma. The higher SiO<sub>2</sub> content is needed because fractional crystallization alone will not sufficiently raise the SiO<sub>2</sub> content to the levels observed in the Karymshina Caldera rocks. However, there must also be large amounts of fractional crystallization to obtain the high SiO<sub>2</sub> levels observed, which would occur in a long-lived magma chamber with a crystalline mush (Bachmann & Bergantz, 2008). Finally, in the shallow crust where the crystalline mush would most likely reside, incorporation of recycled and remelted material would occur, including a small amount of hydrothermally-altered crust with high SiO<sub>2</sub> contents. This hydrothermally-altered crust must have been incorporated into the magma to allow for the final increase in SiO<sub>2</sub> content to bring the magma to the composition observed. It would also account for the normal to low  $\delta^{18}\text{O}$  values of the zircons and normal  $\delta^{18}\text{O}$  values as compared to the high  $\delta^{18}\text{O}$  values of pre-caldera basalts and dacites.

## *Conclusions*

The generation of HSR magma at Karymshina Caldera is most likely due to a combination of magma intrusion into a deep crustal hot zone and fractional crystallization of a large, shallow magma body. In addition, at shallow depths, a small amount of hydrothermally-altered crustal rock with high SiO<sub>2</sub> content must also have been incorporated into the magma. The two eruptive periods, one forming the caldera at 1.78 Ma and one consisting of the post-caldera extrusions from 0.5-0.8 Ma would indicate the presence of a long-lived magma chamber, which is consistent with the idea of a large magma body undergoing fractional crystallization (Bachmann & Bergantz, 2008). The post-caldera extrusions appear to be directly evolved from the caldera-forming ignimbrites or along a mixing trend with the ignimbrites and an unknown higher-SiO<sub>2</sub> magma, although rhyolite-MELTS modeling could not produce the extrusion compositions. The presence of hot springs in the area, along with nearby volcanism, indicate that a magma body may still be present and crystallizing beneath the caldera. The hot springs may also be simply due to higher heat flux in the caldera from previous volcanism and nearby magma bodies. The compositions of the caldera-forming ignimbrites and the post-caldera extrusions show a high degree of homogeneity, which would also be consistent with extraction of a melt from a crystalline mush. A lack of topographical expression of the caldera still presents a problem, but may be due to a combination of erosion by glaciers during the last glacial maximum and high rates of erosion during modern times.

## REFERENCES CITED

- Annen C, Sparks RSJ (2002) Effects of repetitive emplacement of basaltic intrusions on thermal evolution and melt generation in the crust. *Earth Planet Sci Lett* 203:937-955
- Annen C, Blundy JD, Sparks RSJ (2006) The Genesis of Intermediate and Silicic Magmas in Deep Crustal Hot Zones. *J Petrol* 47:505-539
- Auer S, Bindeman I, Wallace P, Ponomareva V, Portnyagin M (2009) The origin of hydrous, high- $\delta^{18}\text{O}$  voluminous volcanism: diverse oxygen isotope values and high magmatic water contents within the volcanic record of Klyuchevskoy volcano, Kamchatka, Russia. *Contrib Mineral Petrol* 157:209-230
- Bachmann O, Bergantz GW (2004) On the origin of crystal-poor rhyolites: Extracted from batholithic crystal mushes. *J Petrol* 45:1565-1582
- Bachmann O, Bergantz GW (2008) Rhyolites and their source mushes across tectonic settings. *J Petrol* 49:2277-2285
- Best MG, Christiansen EH (1997) Origin of broken phenocrysts in ash-flow tuffs, *Geol Soc Am Bull* 109:63-73
- Bianchi I, Agostinetti NP, De Gori P, Chiarabba C (2008) Deep structure of the Colli Albani volcanic district (central Italy) from receiver functions analysis. *J Geophys Res* 113:B09313
- Bindeman IN, Valley JW (2002) Oxygen isotope study of the Long Valley magma system, California: isotope thermometry and convection in large silicic magma bodies. *Contrib Mineral Petrol* 144:185-205
- Bindeman IN, Ponomareva VV, Bailey JC, Valley JW (2004) Volcanic arc of Kamchatka: a province with high- $\delta^{18}\text{O}$  magma sources and large-scale  $^{18}\text{O}/^{16}\text{O}$  depletion of the upper crust. *Geochim Cosmochim Acta* 68:841-865
- Bindeman IN (2005) Fragmentation phenomena in populations of magmatic crystals. *Am Mineral* 90:1801-1815
- Bindeman IN, Schmitt AK, Valley JW (2006) U-Pb zircon geochronology of silicic tuffs from the Timber Mountain/Oasis Valley caldera complex, Nevada: rapid generation of large volume magmas by shallow-level remelting. *Contrib Mineral Petrol* 152:649-665
- Bindeman I (2008) Oxygen isotopes in mantle and crustal magmas as revealed by single crystal analysis. *Min Soc Am, Rev Mineral Geochem* 69:445-478

- Bindeman IN, Fu B, Kita NT, Valley JW (2008) Origin and Evolution of Silicic Magmatism at Yellowstone Based on Ion Microprobe Analysis of Isotopically Zoned Zircons. *J Petrol* 49:163-193
- Bindeman IN, Leonov VL, Izbekov PE, Ponomareva VV, Watts KE, Shipley NK, Perepelov AB, Bazanova LI, Jicha BR, Singer BS, Schmitt AK, Portnyagin MV, Chen CH (2010) Large-volume silicic volcanism in Kamchatka: Ar-Ar and U-Pb ages, isotopic, and geochemical characteristics of major pre-Holocene caldera-forming eruptions. *J Volcanol Geotherm Res* 189:57-80
- Bowen NL (1928) *The Evolution of Igneous Rocks*. Dover Publications, New York
- Braitseva OA, Ponomareva VV, Sulerzhitsky LD, Melekestsev IV, Bailey J (1997) Holocene key-marker tephra layers in Kamchatka, Russia. *Quatern Res* 47:125-139
- Cathey HE, Nash BP (2009) Pyroxene thermometry of rhyolite lavas of the Bruneau-Jarbidge eruptive center Central Snake River Plain. *J Volcanol Geotherm Res* 188:173-185
- Chesley JT, Ruiz J (1998) Crust-mantle interaction in large igneous provinces: Implications from the Re-Os isotope systematics of the Columbia River flood basalts. *Earth Planet Sci Lett* 154:1-11
- Duggen S, Portnyagin M, Baker J, Ulfbeck D, Hoernle K, Garbe-Schönberg D, Grassineau N (2007) Drastic shift in lava geochemistry in the volcanic-front to rear-arc region of the Southern Kamchatkan subduction zone: Evidence for the transition from slab surface dehydration to sediment melting. *Geochim Cosmochim Acta* 71:452-480
- Eichelberger JC, Izbekov PE, and Browne BL (2006) Bulk chemical trends at arc volcanoes are not liquid lines of descent. *Lithos* 87:135-154
- Ellis SM, Wilson CJN, Bannister S, Bibby HM, Heise W, Wallace L, Patterson N (2007) A future magma inflation event under the rhyolitic Taupo volcano, New Zealand: Numerical models based on constraints from geochemical, geological, and geophysical data. *J Volcanol Geotherm Res* 168:1-27
- Faure G, Mensing TM (2005) *Isotopes: Principles and Applications (Third Edition)*. John Wiley & Sons, Inc., New Jersey.
- Geyer A, Marti J (2008) The new worldwide collapse caldera database (CCDB): A tool for studying and understanding caldera processes. *J Volcanol Geotherm Res* 175:334-354

- Gualda GAR, Ghiorso MS, Lemons RV, Carley TL (2011) Rhyolite-MELTS: A modified calibration of MELTS optimized for silica-rich, fluid-bearing magmatic systems. *J Petrol* (In Press)
- Halliday AN, Davidson JP, Hildreth W, Holden P (1991) Modelling the petrogenesis of high Rb/Sr silicic magmas. *Chem Geol* 92:107-114
- Heit B, Sodoudi F, Yuan X, Bianchi M, Kind R (2007) An S receiver function analysis of the lithospheric structure in South America. *Geophys Res Lett* 34:L14307.
- Hughes GR, Mahood GA (2008) Tectonic controls on the nature of large silicic calderas in volcanic arcs. *Geology* 36:627-630
- Jellinek AM, DePaolo DJ (2003) A model for the origin of large silicic magma chambers: precursors of caldera-forming eruptions. *Bull Volcanol* 65:363-381
- Kepezhinskas P, McDermott F, Defant MJ, Hochstaedter A, Drummond MS, Hawkesworth CJ, Koloskov A, Maury RC, Bellon H (1997) Trace element and Sr-Nd-Pb isotopic constraints on a three-component model of Kamchatka Arc petrogenesis. *Geochim Cosmochim Acta* 61: 577-600
- Leonov VL, Rogozin AN (2007) Karymshina, a Giant Supervolcano Caldera in Kamchatka: Boundaries, Structure, Volume of Pyroclastics. *J Volcanol Seismol* 1:296-309
- Mahood GA, Ring JH, Manganelli S, McWilliams MO (2010) New  $^{40}\text{Ar}/^{39}\text{Ar}$  ages reveal contemporaneous mafic and silicic eruptions during the past 160,000 years at Mammoth Mountain and Long Valley caldera, California. *Geol Soc Am Bull* 122:396-407
- Mason BG, Pyle DM, Oppenheimer C (2004) The size and frequency of the largest explosive eruptions on Earth. *Bull Volcanol* 66:735-748
- Nizkous I, Kissling E, Sanina I, Gontovaya L, Levina V (2007) Correlation of Kamchatka Lithosphere Velocity Anomalies with Subduction Processes. In: Eichelberger J, Gordeev E, Izbekov P, Kasahara M, Lees J, (eds) *Volcanism and Subduction: The Kamchatka Region*, *Geophys Monogr Ser*, vol 172, AGU, Washington D.C., 97-106
- Ponomareva V, Melekestsev I, Braitseva O, Churikova T, Pevzner M, Sulerzhitsky L (2007) Late Pleistocene-Holocene Volcanism on the Kamchatka Peninsula, Northwest Pacific Region. In: Eichelberger J, Gordeev E, Izbekov P, Kasahara M, Lees J, (eds) *Volcanism and Subduction: The Kamchatka Region*; *Geophys Monogr Ser*, vol 172, AGU, Washington D.C., 165-198

- Portnyagin M, Hoernle K, Plechov P, Mironov N, Khubunaya S (2007) Constraints on mantle melting and composition and nature of slab components in volcanic arcs from volatiles (H<sub>2</sub>O, S, Cl, F) and trace elements in melt inclusions from the Kamchatka Arc. *Earth Planet Sci Lett* 255:53-69
- Portnyagin M, Hoernle K, Savelyev D (2009) Ultra-depleted melts from Kamchatkan ophiolites: Evidence for the interaction of the Hawaiian plume with an oceanic spreading center in the Cretaceous?. *Earth Planet Sci Lett* 287:194-204
- Rapp RP, Watson EB (1995) Dehydration melting of metabasalt at 8-32 kbar: Implications for continental growth and crust-mantle recycling. *J Petrol* 36:891-931
- Scholl D (2007) Viewing the Tectonic Evolution of The Kamchatka-Aleutian (KAT) Connection With an Alaska Crustal Extrusion Perspective. In: Eichelberger J, Gordeev E, Izbekov P, Kasahara M, Lees J, (eds) *Volcanism and Subduction: The Kamchatka Region*; *Geophys Monogr Ser*, vol 172, AGU, Washington D.C., 3-35
- Shane P, Nairn IA, Smith VC (2005) Magma mingling in the ~50 ka Rotoiti eruption from Okataina Volcanic Centre: implications for geochemical diversity and chronology of large volume rhyolites. *J of Volcanol Geotherm Res* 139:295-313
- Sheimovich VS, Khatskin SV (1996) Rhyodacitic magmatic formation of southeastern Kamchatka. *Volcanol Seismol* 5:99-105
- Sheimovich VS, Golovin DJ (2003) Age of silicic volcanic rocks in the Bolshoy Banny springs. *Volcanol Seismol* 1:21-25
- Sheppard SM, Valley JW, Taylor H, O'Neil JR (1986) Igneous Rocks; III, Isotopic case studies of magmatism in Africa, Eurasia, and oceanic islands. *Rev Mineral* 16:319-371
- Shervais JW, Vetter SK (2009) High-K alkali basalts of the Western Snake River Plain (Idaho): Abrupt transition from tholeiitic to mildly alkaline plume-derived basalts. *J Volcanol Geotherm Res* 188:141-152
- Taran YA, Pokrovsky BG, Volynets ON (1997) Hydrogen isotopes in hornblendes and biotites from Quaternary volcanic rocks of the Kamchatka-Kurile arc. *Geochem J* 31:203-221
- Turner S, McDermott F, Hawkesworth C, Kepezhinskas P (1998) A U-series study of lavas from Kamchatka and the Aleutians: constraints on source composition and melting processes. *Contrib Mineral Petrol* 133:217-234
- Volynets O (1994) Geochemical types, petrology, and genesis of Late Cenozoic volcanic rocks from the Kurile-Kamchatka island-arc system. *Int Geol Rev* 36:373-405

Watts KE, Leeman WP, Bindeman IN, Larson PB (2010) Supereruptions of the Snake River Plain: Two-stage derivation of low- $\delta^{18}\text{O}$  rhyolites from normal- $\delta^{18}\text{O}$  crust as constrained by Archean xenoliths. *Geology* 38:503-506

Watts KE, Bindeman IN, Schmitt AK (2011) Large-volume rhyolite genesis in caldera complexes of the Snake River Plain: Insights from the Kilgore Tuff of the Heise Volcanic Field, Idaho, with comparison to Yellowstone and Bruneau-Jarbidge Rhyolites. *J Petrol* 52:857-890